DR. BABASAHEB AMBEDKAR MARATHWADA UNIVERSITY,
AURANGABAD (MS), INDIA

Design and Development of Non-proliferative Diabetic Retinopathy Detection Technique using Image Features Extraction Techniques

by

Sangramsing Kayte

For Partial Fulfillment of the Requirement for the
Award of the Degree
MASTER OF PHILOSOPHY IN COMPUTER VISION

in the

DR. RAMESH R. MANZA
Department of Computer Science and Information Technology

26 October 2013

Declaration of Authorship

I, SANGRTAMSING KAYTE, declare that this thesis titled, 'Non-proliferative Diabetic Retinopathy detection technique using image features extraction techniques' and the work presented in it are my own. I confirm that:

- This work was done wholly or mainly while in candidature for a research degree at this University.
- Where any part of this thesis has previously been submitted for a degree or any other qualification at this University or any other institution, this has been clearly stated.
- Where I have consulted the published work of others, this is always clearly attributed.
- Where I have quoted from the work of others, the source is always given. With the exception of such quotations, this thesis is entirely my own work.
- I have acknowledged all main sources of help.
- Where the thesis is based on work done by myself jointly with others, I have made clear exactly what was done by others and what I have contributed myself.

Signed:

Date: 26 October 2013

DR. BABASAHEB AMBEDKAR MARATHWADA UNIVERSITY,
AURANGABAD-431 004 Maharashtra (India)
Department of Computer Science & Information Technology

Dr. RAMESH R. MANZA
M.Sc.Ph.D, SET, NET, FIETE
Associate Professor,
Office Telephones: 0240-2403316
Cell: +91-9421308853
Department :(Ext-118)
Fax No 91-240-2403317

University Campus
Aurangabad-431004
(Maharashtra) INDIA
Fax No. : +91-0240-2376576
Telegram : BAMUSITY
http://www.manzaramesh.in
E-mail:manzaramesh@gmail.com

CERTIFICATE

This is to certify that the work incorporated in the thesis entitled **"Design and development of Non-proliferative Diabetic Retinopathy detection technique using image features extraction techniques"**. Submitted to Dr. Babasaheb Ambedkar Marathwada University, Aurangabad by **Mr. Sangramsing Nathusing Kayte** for the award of the degree of Master of Philosophy in the subject of Computer Science was carried out by him under my supervision in the Department of Computer Science and IT, Dr. Babasaheb Ambedkar Marathwada University Aurangabad (MS). This work was not previously submitted by him to this or any other University for the award of any Degree, Diploma, Associate ship or any other similar title.

DR. RAMESH R. MANZA
(Research Guide)

Abstract

The work in this Dissertation mainly focuses on the development of an automatic system, for the purpose of detecting anatomical and pathological features in color retinal images, with its application to diagnosis of diabetic related eye diseases.

Diabetes mellitus, a metabolic disorder, has become one of the rapidly increasing health threats both in India and worldwide. The complication of the diabetes associated to retina of the eye is diabetic retinopathy. A patient with the disease has to undergo periodic screening of eye. For the diagnosis, ophthalmologists use color retinal images of a patient acquired from digital fundus camera. Limited number of specialist ophthalmologists in most of the countries motivates the need for computer based analysis of retinal images using image processing techniques. This could reduce the workload of ophthalmologists, also aid in diagnosis, to make measurements and to look for a change in lesions or severity of disease. The present study is aimed at developing an automatic system for the extraction of normal and abnormal features in color retinal images.

The accurate segmentation of optic disc is often an essential prerequisite step in identification of other retinal anatomical and pathological features. Optic disc localization and its exact boundary detection have been addressed in this work. Iterative thresholding method followed by connected component analysis is employed to locate the optic disc and to find its approximate center. Geometric model based implicit active contour is applied to find the exact boundary of the optic disc. The result of optic disc localization could be used to localize macula or fovea, the other retinal anatomical feature. Also, the optic disc is masked during the detection of lesion, that is, hard exudates to avoid false positives. The result of boundary detection could be used to detect early signs of Glaucoma, which is another sight threatening disease.

Maculopathy is one of the sight threatening stages of diabetic retinopathy. Onset of exudates in the macular region is indicator of macular edema. Manually, severity of maculopathy is decided based on the distance of exudates from the center of macula. As the manual method is highly subjective, an automatic maculopathy detection and severity level grading into mild, moderate and severe is presented. Hard exudates are detected using a K-Means clustering followed by morphological reconstruction.

The sample image data used to validate the system was comparable with the manual graders with regard to severity of the disease. A user interface is also provided for speedy analysis of large number of retinal images during mass screening.

Acknowledgements

Firstly, my gratitude goes to my research guide Dr. Ramesh R. Manza, who was the source of encouragement and motivation during the whole work. His advice, useful hints, indications, suggestions and solution to bottleneck problems encountered during this work are just immensurable. I owe a deep thank to him for directing my research work with extreme competence without which I would not have been able to accomplish this research work.

I am grateful to Dr. K. V. Kale, Professor and Head, Department of Computer Science and Information Technology, Dr. Babasaheb Ambedkar Marathwada University, Aurangabad for his support, encouragement and administrative help.

My Sincere thanks to Dr. S. C. Mehrotra, **Dr. Bharti W. Gawali**, for their encouragement and academic guidance.

I specially thank Mr. Siddhartha Dabhade, Mrs. Manjiri Patwari, and Mr.Bharatratna Gaikwad, for their support and encouragement and to bring out the best in research work.

I thank the university authorities for their supports and proper communication.

The words cannot truly express the gratitude that I owe to my parents, my parent's father Mr.Nathusing Kayte and mother Naginabai kayte, my beloved brother Mr.Charansing Kayte and his wife Kiran Kayte, my Brother Mr.Jaypalsing Kayte and his wife Namrata Kayte, who gave effortlessly their love, support and prayers throughout my academic career.

Contents

List of Figures

List of Tables

Abbreviations

ACM	Active Contour Model
CLAHE	Contrast Limited Adaptive Histogram Equalization
CSME	Clinically Significant Macular Edema
DD	Disc Diameter
DRIVE	Digital Retinal Images for Vessel Extraction
ETDRS	Early Treatment of Diabetic Retinopathy Study
GFR	Gabor Filter Response
GLCM	Gray Level Co-occurrence Matrix
GUI	Graphical User Interface
HIS	Hue Saturation and Intensity
IOP	Intra Ocular Pressure
KMC	Kasturba Medical College
MFR	Matched Filter esponse
NPDR	Non Proliferative Diabetic Retinopathy
PDR	Proliferative Diabetic Retinopathy
RGB	Red Green Blue
ROC	Receiver Operating Characteristics
STARE	Structured Analysis of Retina
WHO	World Health Organization

Chapter 1

Introduction

Recent advances in digital imaging and computing power have made it possible to use data provided from medical images in new and revolutionary ways. This has also led to considerable interest in the development of automatic medical diagnosis systems to improve the services provided by the medical community. These systems aid physician's to diagnose, measure important anatomical structures, monitor changes by comparing sequential images and plan for the better treatment. They also relieve physicians of repetitive work, decreases fatigue and increases efficiency in work.

In clinical ophthalmology, colour retinal images acquired from digital fundus camera are widely used for the detection and diagnosis of diseases related to eye, hypertension and various vascular disorders. Of the many complications of diabetes, visual impairment is perhaps the most feared. Mainly the distressing are in the retina leading to a condition called retinopathy. Diabetic retinopathy is a disorder of the retinal vasculature that eventually develops to some degree in nearly all patients with long standing diabetes mellitus [1]. According to World Health Organization (WHO), number of adults with diabetes in the world would increase alarmingly from 135 million in 1995 to 300 million in 2025. In India, this increase is greatest that is 95% [2]. Diabetic retinopathy is one of the major causes of blindness in the working age population around the world. The prevalence of retinopathy varies with the age of onset of diabetes and the duration of the disease: in younger patients (below 30 years of age) the prevalence of retinopathy is minimal during the first 5 years but increases to greater than 95% after 15 years of diabetes [3]. In contrast among patients whose onset of diabetes occur after the age of

30, up to 20% may have signs of retinopathy on presentation with the prevalence in this group rising more slowly to approach 60% after 15 years of diabetes. Unfortunately, because visual loss is often a late symptom of advanced diabetic retinopathy, many patients remain undiagnosed even as their disease is causing severe retinal damage. It is shown that timely diagnosis and referral for management of diabetic retinopathy can prevent 98% of severe visual loss. First step in prevention of the disease is to have a regular diabetic retinopathy screening program. The process involves acquiring the retinal image using standard digital colour fundus camera. The ophthalmologist uses images to aid in diagnosis, to make measurements of the normal anatomical structures, to locate abnormalities and to look for a change in lesions.

Given the number of diabetes patients screened yearly, the number of retinal images generated is large. The high cost of examination and the shortage of ophthalmologists, especially in rural areas, are prominent factors that hamper patients from obtaining regular examinations [3]. Therefore, the need for automated retinal image processing system arises that can screen the initial set of images for any signs of abnormalities. Only those images with lesions can be forwarded to ophthalmologists for further analysis. This could save the workload of ophthalmologists and assist them to analyze a large database of retinal images in a short period of time. A fully automated system can detect early signs of diabetic retinopathy, provide objective assessment, monitor the progression of disease and monitoring of the onset and progression of the disease, as well as analysis of anatomical structures.

1.1 Objectives and Scope

The primary objective of evaluating and managing diabetic retinopathy is to prevent, retard, or reverse visual loss, thereby maintaining or improving vision- related quality of life. In ophthalmology, for diagnosis of diabetic retinopathy, digital colour retinal images are becoming increasingly important. In computer based retinal image analysis system, image processing techniques are used in order to facilitate and improve diagnosis. Manual analysis of the images can be improved and problem of detection of diabetic retinopathy in the late stage for optimal treatment may be resolved.

The automatic detection of landmark anatomical structures and lesions are needed during the mass screening for the detection and diagnosis of diabetic retinopathy. The anatomical structures detection helps in characterizing the detected lesions and in identifying false positives. Lesion detection is essential for monitoring purpose and to classify the severity stages of the disease. Based on these the main objectives of the work are summarized as follows.

To automatically detect the following normal features in retinal image to improve the performance of pathology detection.

- Automatic detection of optic disc boundary
- Automatic detection of macular region
- Automatic detection of retinal blood vessels

To automatically detect lesion, i.e., exudates in retinal images for the early detection of diabetic retinopathy.

To develop an automatic retinal analysis system to classify severity of the disease.

Current techniques of diabetic retinopathy detection and assessment are mostly manual, expensive, and potentially inconsistent requiring highly trained staff to facilitate the process by searching large number of retinal images. It is hoped that the proposed system can assist ophthalmologists to make diagnosis more effective and provide an automatic cost effective tool for the mass screening of retinopathy.

1.2 Dissertation Outline

In this Dissertation, automatic methods to analyze the digital retinal images for detection of diabetic retinopathy are proposed. The overall retinal image analysis system is shown in the Figure 1.1. The system is capable of choosing the diabetic patients who need further examination during the mass screening. It is also able to provide the severity level of maculopathy, a sight threatening complication of diabetic retinopathy. Few of the retinal images acquired during the examination may be of inadequate quality for

manual analysis. Factors that affect the clear visualization of retina are due to operator inexperience with fundus photography, problems in patient focusing and insufficient light reaching retina. In the first stage, such colour retinal images are preprocessed using local contrast enhancement technique. Next, only the green component in the colour image is extracted as it provides the maximum details about structures present in the retinal image.

Once the images have been preprocessed, the landmark anatomical structures: optic disc, fovea and blood vessels are detected. Localization of the optic disc is required as prerequisite for the subsequent stages for identification of other anatomical structures in an image. During the exudates lesion identification, many false positives arise due to other pale objects including light reflections, cotton

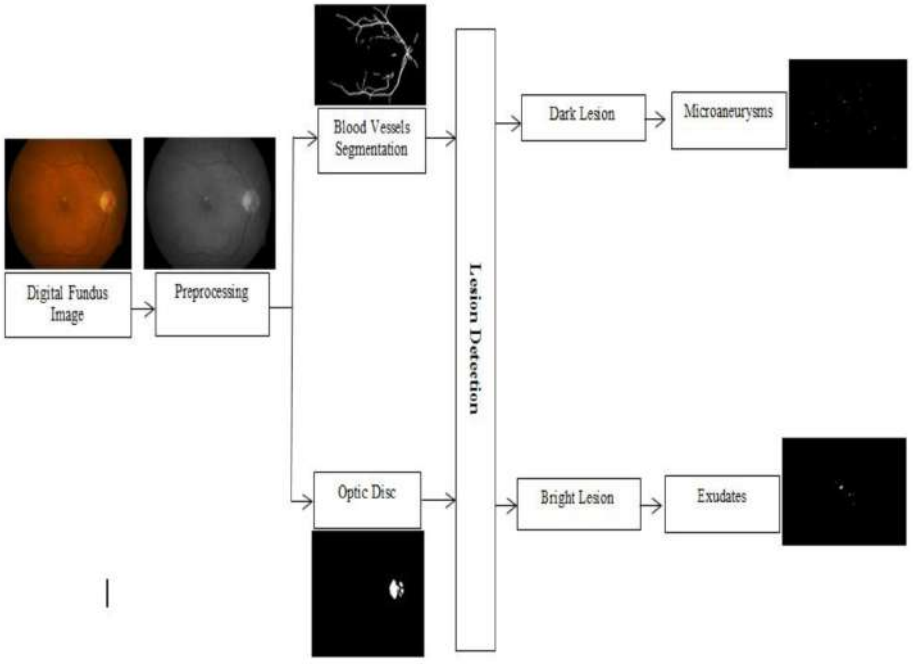

FIGURE 1.1: Outline of the proposed retinal image analysis system

wool spots, and most significantly, the optic disc. The localization and segmentation of optic disc boundary is achieved in two step approach. First, the approximate center of optic disc is detected in the retinal image using iterative thresholding method followed by connected component analysis. It provides baseline in finding out its exact boundaries. Then, the geometric model based implicit active contour is employed to obtain accurate optic disc boundary. Fovea or macula encircling helps establishing statistics regarding lesions position for disease gradation [4]. It is reported in that the distance and position of fovea with respect to the optic disc remains relatively constant. Once the optic disc

is detected, the fovea is localized by finding the darkest region in the image following the prior geometric criteria based on the eye's anatomy.

Automatic segmentation of the vasculature in retinal images is important in the detection of diabetic retinopathy that affects the morphology of the blood vessel tree. The proposed retinal vessel detection method is comprised of two steps. The blood vessels will be oriented along different directions and they also vary in thickness along their length. Initially, Gabor filters tuned to particular frequency and orientation are used to enhance the blood vessels suppressing the background. A bank of twelve Gabor filters with the range of 00 – 1700 degree in 150 degree steps are used to enhance the retinal blood vessels. Filtering involved computationally intensive convolution operation. Therefore, by experimentation it is found that increasing the number of Gabor filters beyond twelve did not result in high increase of vessel detection accuracy [5]. It is also found in the literature that vessel segments lying within 7.50 degree of direction of chosen kernel will respond well. The colour image does not provide much information to distinguish vessels from background. Therefore, the image was decomposed into 3 channels – red, green and blue (each one of them represented in the scale of gray). Only the green channel image is used for further processing as it provided more contrast. It also reduced the computational cost of the algorithm by three fold. Maximum Gabor response image results in enhanced vessels. In the next step, entropy based thresholding based on gray level co-occurrence matrix is employed for the segmentation of the vessel pixels. The performance of the method was tested on two sets of publicly available retinal databases. Then, the accuracy of the method is compared in terms of pixel resolution and image based criteria against a provided pixel-level ground truth dataset.

Hard exudates are abnormal lesions caused by diabetic retinopathy in a diabetic's eye and they are considered to be bright intensity regions in the retinal images. First step in the identification of exudate regions is the detection and masking of optic disc to avoid false positives. The exudates regions are detected using a combination of dynamic clustering and mathematical morphology. The initial candidate exudate regions are obtained by clustering the intensity difference image in the image space. For the fine segmentation of the exudates, morphological reconstruction technique is employed. Finally, the exudate regions are obtained by thresholding the difference between the original image and the reconstructed image. The threshold varies from one image to another, so an entropic thresholding technique is used for the automatic calculation of

optimal threshold. Image based method is employed to verify the diagnostic accuracy of the method. Here each single exudate lesion is regarded as an individual connected region, where this region can be comprised of one or more pixels. Each abnormal retinal image can be segmented into a number of exudate regions. Finally, the performance of the method was validated by the ophthalmologists. Also a standard dataset was used to evaluate the image based exudate detection.

Next stage in the automatic retinal analysis system is to make a decision regarding the severity level of the diabetic maculopathy. The presence and spread of exudates determine the severity of the disease as mild, moderate and severe. Localization of exudates in the area of macular region lead to a condition called Clinically Significant Macular Edema (CSME). If the exudates are very apparent and affect the center of macular region, the fovea centralis, visual function will be significantly and irrevocably damaged. After the detection of macula and exudates, the macular region is identified and it is divided into marker regions. Automatic grading of diabetic maculopathy is done according to the international clinical diabetic macular edema disease severity scale [6]. According to a minimum standard of 80% sensitivity and 95% specificity for the detection of diabetic retinopathy is to be achieved by any method. The result obtained from the proposed work has met the requirement as comparable to human expert. A Graphical User Interface (GUI) has also been developed that can be used by clinicians during the mass screening.

1.3 Organization of the Dissertation

The Dissertation is organized according to the respective identification tasks of the automated retinal image analysis system for the detection of diabetic retinopathy as follows.

Chapter 1

Introduces the background of medical domain. It includes anatomy of the ocular fundus and the landmark retinal structures. Eye complications of diabetes, i.e., retinopathy and its sight threatening stage called maculopathy are discussed. This chapter also provides a literature review on the retinal image analysis systems and algorithms.

Chapter 2

Presents acquisition of retinal image and pre-processing methodologies. The specifications of the retinal images that are used in this work are discussed. Details of retinal images obtained from standard databases are mentioned. In the pre-processing step colour normalization, local contrast enhancement and extraction of green component in the retinal image is described.

Chapter 3

Presents the automatic segmentation of retinal vessels. The properties of the vessels and how they are used to design the Gabor filter is described. A set of Gabor filters oriented along different directions are used to enhance the vessels. It is followed by segmentation of vessel pixels using automatic calculation of threshold. The performance of the method is analyzed and compared with other vessel segmentation approaches.

Chapter 4

Presents the automatic localization of landmark feature of retina, the optic disc. It starts with the detection of approximate center of disc using iterative thresholding and connected component method. Followed by, the segmentation of exact boundary of optic disc based on geometric active contour model. Then the size and location of optic disc is used to identify the macula, the center of ocular fundus.

Chapter 5

Explains the automatic segmentation of exudate lesions. The hybrid method using K-Means clustering for coarse segmentation and mathematical morphology for fine segmentation are discussed. The performance of the method on two different set of databases are presented. The chapter also describes the automatic grading of diabetic maculopathy severity level. Development of the GUI for mass screening of retinopathy and its snap shots are also provided.

Chapter 6

Presents Dissertation conclusions on the basis of analysis and discussion and highlights the contributions of this work. It also includes scope for improvement and future direction of research.

Chapter 2

Literature Review

This chapter provides the details related to basics of medical domain, especially ophthalmology. The anatomy of human eye, ocular fundus and its main anatomical components are briefly explained. Then description about the cause of diabetic retinopathy and maculopathy diseases, their symptoms, complications and risks at the individual level is provided. This chapter also presents a detail literature survey of existing methods on the automatic detection of anatomical structures in retina and current scenario of automatic diagnostic systems. Furthermore, the concepts and techniques used for developing the proposed methods have been presented in this chapter

2.1 Anatomy of Human Eye

Vision is arguably the most used of five senses in the human body. We rely on our eyes to provide most of the information we perceive about the world, so much so, that a significant portion of the brain is devoted entirely for visual processing [7]. The eye is often compared to a camera because of the way it processes light into information understandable by the brain. Both have lenses to focus the incoming light. A camera uses the film to create a picture, whereas the eye uses a specialized layer of cells, called the retina, to produce an image. However the similarity stops here. The eye's ability to focus on a wide range of objects having different sizes, luminosity and contrast at a high speed is more powerful than those of current cameras. Figure 2.1 illustrates a cross section of the human eye and highlights the main components. Light reaches the eye by first

passing through the cornea which filters it, and begins focusing the image. The anterior chamber contains a viscous substance called aqueous hum our that keeps the front of the eye firm and slightly curved. Light travels through the pupil, which compensates for changing light conditions by contracting or relaxing. The muscles responsible for these movements are in the iris. Subsequently, the lens squeezes or stretches to focus the rays of light on the retina. Among the various ocular structures, only the anatomical structures of retina are more relevant to the research work.

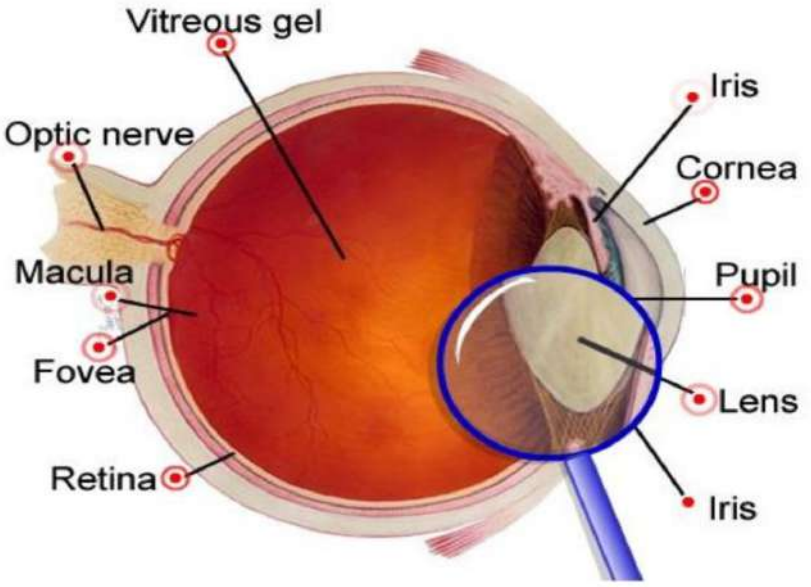

FIGURE 2.1: Anatomy of human eye

The retina is a thin multi-layered sensory tissue that covers the inside wall at the back of eye called fundus. It is covered by millions of photoreceptors (rods and cones). These photoreceptors are responsible for receiving light beams, converting them into electrical impulses and then transmitting these to the brain where they are turned into images. Figure 2.2 illustrates a typical normal retinal fundus image with highlighted regions of fovea, optic disc, blood vessels and macula. The outlying parts of the retina are responsible for peripheral vision while the central area, called macula, is in charge of central vision that allows us to see details and perform tasks that require central vision, for example, reading. The macula is a circular area in the central region of the retina measuring about 4 mm to 5 mm in diameter. A small depression in the center of macula measuring about 1.5 mm in diameter

is called fovea. The fovea corresponds to the region of retina with highest sensitivity. The optic disc is the entry and exit site of blood vessels and optic nerve fibers responsible

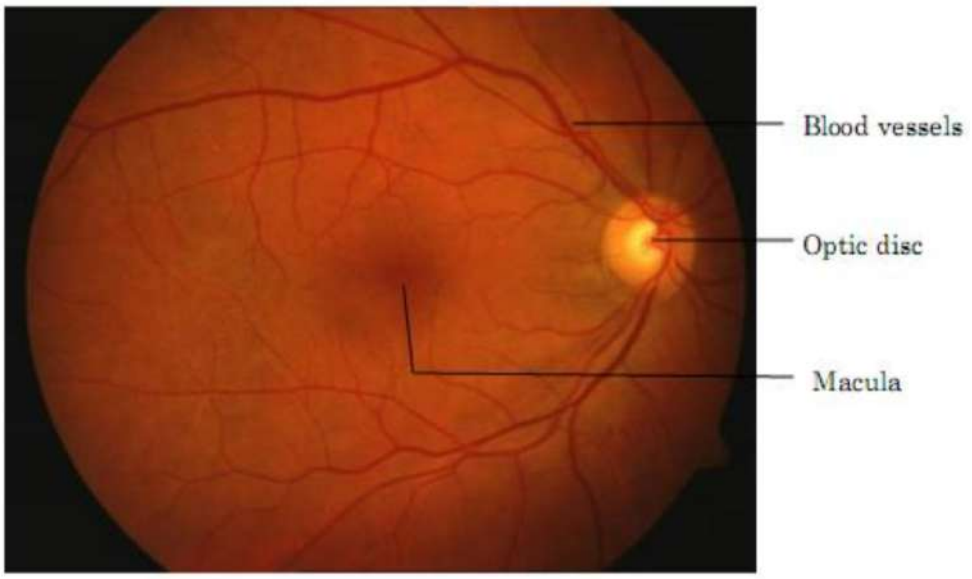

FIGURE 2.2: Anatomical structures of ocular fundus

for transmitting electrical impulses from the retina to the brain. It is a brighter region than the rest of the ocular fundus and its shape will be usually round. The optic disc is approximately 3 mm nasal to the fovea, and it measures about 1.5 mm to 2 mm in diameter. The optic disc contains a central depression called optic cup and its depth varies among different individuals. The retinal blood vessels are derived from the central retinal artery and vein are responsible for nourishing the inner parts of the retina. The following section elucidates the complications of diabetic eye diseases that affect the normal functioning of retina.

2.2 Diabetic Eye Diseases

Diabetes mellitus is a metabolic disorder characterized by chronic hyperglycaemia with disturbances of carbohydrate, fat and protein metabolism resulting from defects in insulin secretion, insulin action, or both [8]. Diabetes has become one of the rapidly increasing health threats both in India and worldwide. One of the most feared complications of diabetes is damage caused to the eye. It is estimated that people with diabetes have a 25 times greater risk of going blind than the non-diabetic population [9]. Diabetic retinal changes are a major cause of visual impairment and thus understanding of this diabetic complication is imposed as a particular health, social and economic problems [10]. The two main complications associated to the retina are diabetic retinopathy and

maculopathy. It is estimated that at any time around 10% of patients with diabetes will have diabetic retinopathy [11]. According to early and complete photocoagulation of the affected area is the only treatment for delaying or preventing the decrease in visual acuity [6].

2.3 Diabetic Retinopathy

Diabetic retinopathy is a vascular disorder occurring due to the combination of micro-vascular leakage and micro-vascular occlusion within the retina [12]. It is primarily classified into Non-Proliferative Diabetic Retinopathy (NPDR) and Proliferative Diabetic Retinopathy (PDR). Typically there are no salient symptoms in the early stages of diabetic retinopathy, but the number and severity predominantly increase with the time. Non proliferative diabetic retinopathy is the most common and may arise at any point in time after the onset of diabetes. Ophthalmologists detect these changes by examining the patient's retina and look for spots of bleeding, lipid exudation, or areas of retinal swelling. Identification and recording of the following abnormalities (see Figure 1.3) will aid in the accurate assessment of retinopathy severity.

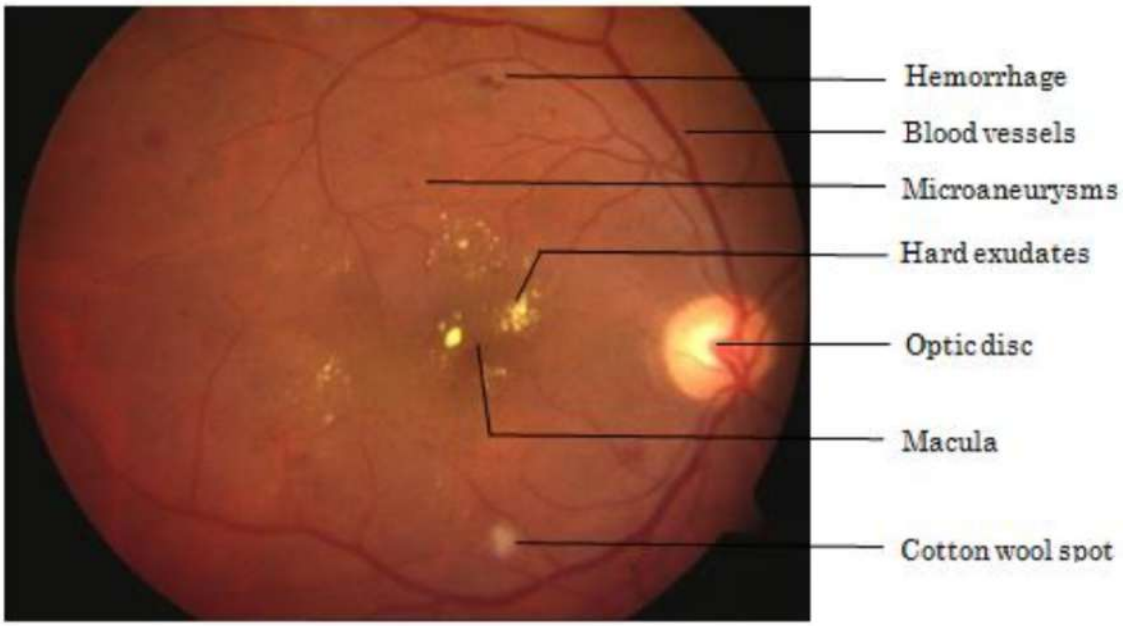

FIGURE 2.3: Anatomical and pathological features in colour retinal image

Microaneurysms: These are the earliest clinical abnormality to be noticed in the eye. These are local swelling of retina capillary and usually appear in isolation or in clusters.

Their size ranges from 10 to 100 microns and are dark red spots that look like tiny hemorrhages [10]. The number of microaneurysms increases as the degree of retinal involvement progresses.

Hemorrhages: Intra-retinal hemorrhages appear when capillaries or microaneurysms rupture and some blood leaks out of these vessels. In Figure 1.3 hemorrhages can be seen as red flame shaped regions.

Hard exudates: Hard exudates represent leak of fluid that is rich in fat and protein from surrounding capillaries and microaneurysms within the retina. These are one of the main characteristics of diabetic retinopathy and appear as random yellowish patches of varying sizes, and shapes.

Soft exudates: These are often called cotton wool spots and are more often seen in advanced retinopathy. These abnormalities usually appear as little fluffy round or oval areas in the retina with a whitish colour, usually adjacent to an area of hemorrhage. Cotton wool spots come about due to the swelling of the surface layer of the retina in the absence of normal blood flow through the retinal vessels. The nerve fibers are injured in a particular location resulting in swelling and appearance of a cotton wool spot.

Proliferative diabetic retinopathy, the advanced stage retinopathy develops in more than 50 percent cases after about 25 years of onset of the disease. Therefore, it is more common in patients with juvenile onset diabetes [13]. The hallmark of PDR is the growth of new blood vessels in the areas where normal capillaries have already closed. These new blood vessels are abnormal and fragile. They grow along the retina and along the surface of the clear, vitreous gel that fills the inside of the eye. By themselves, these blood vessels do not cause symptoms or vision loss. However, they have thin, fragile walls that leak blood resulting in severe vision loss and even blindness can be the end result.

2.4 Diabetic Maculopathy

Diabetic maculopathy is a common complication of diabetes mellitus, characterized by macular edema and frequently accompanied by lipid exudation [14]. Diabetic maculopathy, defined as retinopathy within one disc diameter of the center of the macula is

the major cause of vision loss [15]. One of the morphological characteristics of diabetic retinopathy clinical signs is the onset of retinal hard exudates, which are manifested as whitish- yellowish changes. They are most frequently localized in the area of the macular region, surrounding the zones of retinal edema, although they can also be noticed in other localizations at the posterior pole of the eye fundus. They are a dominant feature in both exudative and mixed types of diabetic maculopathy. If they are very apparent and affect the center of macular region called fovea centralis, visual function is significantly and irrevocably damaged as shown in Figure 2.4. Diabetic maculopathy comprises of two aspects: First is the macular edema in which fluid and lipoproteins accumulate within the retina. Second is the macular ischemia in which there is closure of perifoveal capillaries demonstrable on fundus fluorescein angiography. It is not known to what extent macular ischaemia contributes to the visual loss attributable to diabetic maculopathy and this work is limited to the automatic detection of macular edema and its severity stages.

FIGURE 2.4: Normal vision (left) and same scene viewed by person with diabetic maculopathy (right)

2.5 Literature Review

Recent advances in technology have led to the development of digital imaging systems offering very high-resolution images that are sufficient for most clinical scenarios [16][17]. In ophthalmology, retinal digital imaging provides a permanent, high quality record of

the appearance of the retina with application for screening program of diabetic retinopathy [18]. Digital retinal images can be subjected to image analysis to perform objective quantitative analysis of fundus images and has the potential for automated diagnosis to aid in decision making. Retinal image analysis is a complicated task, particularly because of the variability of the images in terms of the colour, the morphology of the retinal anatomical pathological structures and the existence of particular features in different patients, Which may lead to an erroneous interpretation. This has led to the development of many retinal image analysis methods. Retinal images are usually processed in an algorithmic sequence, with the output of one stage forming the input to the next. Typical sequence may consist of one or more preprocessing procedures followed by image segmentation, feature extraction and classification stages. This literature survey reviews the work related to digital retinal image analysis in the automated diagnosis of diabetic retinopathy with emphasis on detection of normal and abnormal features in the digital colour retinal image.

2.5.1 Vessel segmentation methods

The segmentation and measurement of the retinal vasculature is of primary interest in the diagnosis and treatment of a number of ophthalmologic conditions [5][19]. The accurate segmentation of the retinal blood vessels is often an essential prerequisite step in the identification of retinal anatomy and pathology. In addition, the segmentation of the vessels is useful for registration of patient images obtained at different times [20][22]. Existing vessel extraction techniques and algorithms can be classified into four main approaches as follows [21].

Matched filter approaches: Matched filtering involves convolution of the image with multiple filters for extraction of objects of interest [23]. In a two-dimensional kernel was proposed for segmentation of the vasculature. The profile of the filter is designed to match that of a blood vessel, which typically has a Gaussian or a Gaussian derivative profile [24]. The kernel is typically rotated in 30 to 45 degrees increments to fit into vessels of different orientations [25]. The highest Matched Filter Response (MFR) is selected for each pixel and is typically thresholded to provide a vessel image [26]. As noted by several authors a MFR method is effective when used in conjunction with additional processing techniques. However, the convolution kernel may be quite large

and needs to be applied at several rotations resulting in a computational overhead, which may reduce the performance of the overall segmentation approach. In addition, the kernel responds optimally to vessels that have the same standard deviation of the underlying Gaussian function specified by the kernel [27]. As a consequence, the kernel may not respond to vessels that have a different profile. The retinal background variation and low contrast of the smaller vessels also increases the number of false responses around bright objects such as exudates and reflection artifacts [28]. Several authors have proposed refinements and extensions which address many of these problems. In the local and region-based properties are used to segment blood vessels in retinal images [8]. The method examined the matched filter response image using a probing technique. The technique classified pixels in an area of response image as vessels and non-vessels by iteratively decreasing the threshold [27]. In each of the iteration, the probe examined the region-based attributes of the pixels in the tested area and segmented the pixels classified as vessels.

Vessel tracking approaches: Vessel tracking algorithms segment a vessel between two points [29]. Unlike the previously described techniques for vasculature segmentation they work at the level of a single vessel rather than the entire vasculature [30]. A vessel tracking approach typically steps along the vessel. Here the center of the longitudinal cross-section of vessel is determined with various properties of the vessel including average width and toruosity measured during tracking [31]. The main advantage of vessel tracking methods is that they provide highly accurate vessel widths, and can provide information about individual vessels that is usually unavailable using other methods. Unfortunately, they require the starting point, and usually the end point, of a vessel to be defined by a user and are thus, without additional techniques, of limited use in fully automated analysis. In addition, vessel-tracking techniques may be confused by vessel crossings and bifurcations and often tend to terminate at branch points.

Classifier based approaches: Artificial neural networks have been extensively investigated for segmenting retinal features such as the vasculature [4]. The operation of a neural network is analogous to that of a matched filter. Both take sub windows of the image as input and return a probability measure as output. Two studies, both using the back-propagation algorithm, have detected and segmented the retinal vasculature [32]. Detection involves classifying sub windows as containing vessels or not [33]. Segmentation involves classification of individual vessel and non-vessel pixels. In images

are preprocessed with principal component analysis to reduce background noise by reducing the dimensionality of the data set and then applied a neural network to identify the pathology [34]. They reported overall sensitivity and specificity of 83.3% and 91%, respectively. The result of the approach was compared with an experienced ophthalmologist manually mapping out the location of the blood vessels in a random sample of seventy three 2020 pixel windows and requiring an exact match between pixels in both images [33]. The neural networks researched by used 2020 pixel sub windows. Nine thousands of these sub windows were marked for neural learning validation. Generalization assessment over 1200 unseen sub windows resulted in a sensitivity of 91.7%. One of the advantages that make neural networks attractive in medical image segmentation is its ability to use nonlinear classification boundaries obtained during the training of the network and ability to learn. However, one of the disadvantages of it is that they need to be trained every time whenever a new feature is introduced to the network and another limitation is the necessity for configuring the network with training data or a gold standard. This gold standard data set consists of a number of images whose vascular structure must be precisely marked by an ophthalmologist. However, as noted by there is significant disagreement in the identification of vessels even amongst expert observers [35]. Morphological approaches: Morphological image processing exploits features of the vasculature shape that are known a priori, such as it being piecewise linear and connected [36]. Algorithms that extract linear shapes can be very useful for vessel segmentation. In a vessel segmentation algorithm from retinal angiography images based on mathematical morphology and linear processing was presented [37]. A unique feature of the algorithm is that it uses a geometric model of all possible undesirable patterns that could be confused with vessels in order to separate vessels from them [38]. The strength of the algorithm comes from the combination of mathematical morphology and differential operators in the segmentation process [38]. In linear bright shapes and basic features are extracted using mathematical morphology operators and vessels are extracted using curvature differentiation and laplacian filter. Utilized morphological closing to help identify veins in the automated grading of venous beading by filling in any holes in the silhouette of the vein created during the processing procedure. The main disadvantage of exclusively relying upon morphological methods is that they do not exploit the known vessel cross-sectional shape. Also, this approach works well on normal retinal images with uniform contrast but suffers from noise due to pathologies within the retina of eye [39].

2.5.2 Optic disc and Macula detection methods

The location of the optic disc is important in retinal image analysis. For example, it is used for vessel tracking, as a reference length for measuring distances in retinal images and for registering changes within the optic disc region due to disease [47]. In case of diabetic retinopathy lesions identification removing the false positive optic disc region leads to improved lesion diagnosis performance [48]. The measurement of varying disc diameter is used in the detection of glaucoma. Existing methods and their drawbacks for the localization and boundary detection of the optic disc is as follows.

Optic disc localization: There have been few works on locating the optic disc in retinal images based on the gray level variation in the optic disc region [49]. Here, the optic disc was localized by identifying the largest cluster of bright pixels [33]. These algorithms proved to be simple, fast and reasonably robust for optic disc localization in normal retinal images with negligible variation between images [50]. However, an optic disc obscured by blood vessels or only partially visible will be misidentified using these methods. Also, these methods did not find the center of the optic disc [33].

In few works, characteristics of the optic disc like intensity, morphology and colour were investigated for localizing the disc in the presence of distracters [51]. Used an 8080 pixel sub-image to evaluate the intensity variance of adjacent pixels [50]. The point with the largest variance was assumed to be the center of the optic disk [54]. The assumption was that visible signs of disease such as exudates will have a lower intensity variance than the optic disk [52]. The authors reported 99.1% sensitivity in localizing the center of the optic disk in images with little or no visible signs of lesions [53]. However, reported the misidentification of the optic disc using this algorithm in retinal images with large number of white lesions, light artifacts or strongly visible choroid vessels [55],[51]. Proposed a similar technique using a 110110 pixel template image obtained by averaging the optic disk region in 25 retinal images [56]. They reported of successfully localizing the approximate center of the optic disk in all of 75 images considered [57]. In fact, the authors made an assumption to locate the optic disc from those retinal images with no visible symptoms. The Hough transform has been investigated by a number of authors for the localization of the optic disc. The underlying principle used to identify the optic disc was to consider that a retinal image is comprised of an infinite number of potential circles which pass through a number of edge points. The edge points are derived from

edge information extracted by applying one of several available edge detection algorithms [54]. The Hough transform determines which of these potential circles intersect with the greatest number of circles in the image. Used a circular Hough transform after edge detection to localize the optic disc in the red colour channel. The first stage searched for an optic disc candidate region defined as a 180180 pixel region that included the brightest 2% of gray level values [55]. A Sobel operator was then applied to detect the edge points of the candidate region and the contours were then detected by means of the circular Hough transform. Proposed a combination of a Hough transform and steerable filters to automatically detect the location and size of the disk. These kinds of approaches are quite time consuming and rely on conditions regarding the shape of the optic disc that are not always met. Moreover, edge detection algorithms often fail to provide an acceptable solution due to the fuzzy boundaries, inconsistent image contrast or missing edgefeatures.Principal components analysis has also been used as a means of extracting common features of retinal images including the optic disk and blood vessels [58].

The likelihood of a candidate region being an optic disk was determined by comparing the characteristics of the optic disk extracted from a training image to those derived from an unseen image [33]. Reported the correct localization of the optic disc with sensitivity of 99% in 89 images. Few methods have reported a technique for locating the optic disc using a geometrical parametric model [59]. According to the retinal vessels originating from the optic disc follows a similar directional pattern in all images [60]. Reported of correctly identifying optic disc with 89% sensitivity using a fuzzy convergence algorithm. Their method finds the strongest vessel network convergence as the primary feature for detection using blood vessel binary segmentation, the disc being located at the point of vessel convergence. In these works, the authors did not address the optic disc boundary localization and also segmentation and tracking of vessels itself is a difficult task [61]. Localized the optic disc using a combination of two procedures including a Hausdorff based template matching technique on the edge map, guided by a pyramidal decomposition technique. The edge maps were calculated using canny edge detection and therefore the low and high hysteresis thresholds must bedefined properly. The drawback was that a priori information of the image characteristics and whether the input image is centered on macula or on optic disc had to be provided making it semiautomatic.

Optic disc boundary segmentation: Optic disc contour segmentation is usually performed after localizing disc and it is a non-trivial problem [62]. Described an approach using colour space transformation and morphological filtering techniques for disc localization. The optic disc was first localized using the luminance channel of the hue-luminance-saturation colour space and a thresholding operation was applied to determine the approximate locus of the optic disk. The precise contour of the disk was then determined, using watershed transform. The contour of the optic disc was identified in 27 of the 29 images often with slight distortion of the contour due to outgoing vessels or low contrast.

Few works have investigated the parametric active contour model to detect the boundary of optic disc [63]. Investigated applying morphological operator followed by an active contour to segment the disc [50]. Presented two key extensions in the use of gradient vector flow snakes for optic disc segmentation. Here, the optic disc was first localized using template matching [63]. Secondly, colour morphological processing was used to obtain a more homogeneous inner disk area, which increased the accuracy of the snake initialization [50]. In these methods the parametric active contours depend much on image gradient and less sensitive to location of initial contour resulting in reduced performance weak optic disc boundaries.

Fovea localization: Temporal to the optic nerve head is the fovea (or macula), which appears darker in colour and has no blood vessels present in the center [64]. The fovea lies at the center of the macula and is the part of the retina that is used for fine vision. The fovea was detected by looking at the non-vessel area and intensity variation [33]. In the location of the fovea was chosen as the position of maximum correlation between a model template and the intensity image, obtained from the intensity-hue-saturation transformation. In these methods, foveal localization was particularly affected if there was poor centration of the fovea in the image. Detected the foveal region using model-based methods. They estimated the position of the fovea by extracting the points on the main blood vessels by a modified active model, and fitting a parabola curve with the optic disc as the center. Fovea is then located at 2 disc diameters from the optic disc on the main axis of the parabola.

In the proposed work a new approach for the automatic localization and accurate boundary detection of the optic disc is presented. Iterative thresholding method followed by

connected component analysis is employed to locate the approximate center of the optic disc. Then geometric model based implicit active contour model is applied to find the exact boundary of the optic disc. The method is evaluated against a carefully selected database of 148 retinal images and compared with the human expert. The center of optic disc is found with an accuracy of 99.3%. The mean sensitivity of 90.67%(standard deviation of 5) is achieved for correct boundary segmentation. The fovea is located based on its distance from the center of the optic disc. To find the exact center of macula called foveola, a search area is formed to find darkest non-vessel region. The method was able to achieve 96.6% sensitivity for locating the center of fovea.

2.5.3 Hard exudates detection methods

Exudates are one of the most commonly occurring lesions in diabetic retinopathy. They are associated with patches of vascular damage with leakage. The size and distribution of exudates may vary during the progress of the disease. The detection and quantification of exudates will significantly contribute to the mass screening and assessment of diabetic retinopathy.

In one of the earliest method by fundus transparency was imaged [65], digitized, and then pre-processed, to reduce shade variations in the image background and enhance the contrast between the background and the exudate lesions. Exudates were then separated from the background on a gray level basis. The proposed technique required user intervention for selecting the threshold value. Most exudates show higher gray level values compared to the nearby retinal background, some smaller exudates have about the same intensity as the background of the retinal making it unlikely for simple global thresholding techniques to present a satisfactory result [54]. Therefore, introduced a dynamic thresholding algorithm, which calculated every pixel's threshold according to its local histogram. In this way, the images were firstly divided into 64 64 pixel patches and then the local threshold of each patch was obtained using its histogram feature. Then, the dynamic threshold of every pixel was found using interpolation of the local thresholds of four neighboring patches which include that pixel. These methods also detected other type of lesions like cotton wool spots along with exudates. Classifier based methods were used to separate exudates from other lesions [28]. In a minimum distance discriminant classifier was used to categorize each pixel into yellow lesion or

non-lesion class [56]. This work proposed to differentiate yellow lesions from red lesions, but it involved misclassification of other yellowish lesions at the same time [66]. The image-based diagnostic accuracy of this approach was reported as 100% sensitivity and 70% specificity [56].

Used a combination of template matching, region growing and thresholding techniques for preliminary lesion detection [28]. Then they used Bayesian classifier to classify the yellow lesions into exudates, cotton wool spots and noise. The classification performance for this stage was only 62% for exudates and 52% for the cotton wool spots [67]. Presented a domain knowledge based approach to detect exudates. Dynamic clustering was used to determine lesion clusters. Then, domain knowledge was applied to identify true exudates [68]. Detected the candidate exudates region by using a combination of region growing and adaptive intensity thresholding [67]. In the spectrum feature center of exudates and background are computed and then the distance from each pixel to class center is calculated. The pixel is classified as exudate if it falls within the minimum distance.

Neural networks and fuzzy clustering have also been exploited to classify the retinal abnormalities in a few studies the retinal images were broke down into small squares and are inputted to a back propagation neural network [44]. In the image was segmented depending on colour using Fuzzy C-means clustering [69]. Then, 18 different features were inputted to a three layer neural network. They reported detection with 93% sensitivity and 94.1% specificity in terms of lesion based classification [70] [69]. Another neural network based exudate detection research was conducted by [44]. The network was trained to distinguish exudates from drusen based on 1616 pixel patches. They introduced a hierarchical feature selection method, based on sensitivity analysis to distinguish the most relevant features [51]. They reported to have achieved 91% in lesion-based classification applied to a relatively small number of images. Applied a recursive region growing technique using selected threshold values in gray level images [33]. In this work it was supposed that the processed retinal images are only including exudates, hemorrhages and microaneurysms and other lesions for example cotton wool spots were not considered. The authors have reported an accuracy of 88.5% sensitivity and 99.7% specificity for the detection of exudates. Exudates were also detected using morphological techniques [37]. In exudates were identified according to their gray level

variation [71]. After initial localization [72], the exudates contours were subsequently determined by mathematical morphology techniques [37]. The candidate exudate regions are initially found based on the initial threshold value. The second threshold represents the minimum value, by which a candidate must differ from its surrounding background pixels. They have reported an accuracy of 92.8% against a set of 15 abnormal retinal images. In the proposed work, the hard exudates detection is performed in two successive steps. Initially the possible exudates regions are coarse segmented by k-means clustering technique to separate possible exudate regions from the background in the image space. Next morphological reconstruction technique is applied to correctly segment the exudate regions. The method achieved an image based sensitivity of 98% for exudate detection on set of 130 images and the result is also validated by ophthalmologists.

2.5.4 Automatic retinal screening systems

With the ever increasing diabetic population and the availability of fundus images in digital format, there is a need for computer based retinal screening systems. It is assumed that an automatic screening system would save the workload of ophthalmologists and aid in the diagnosis [73]. Evaluated the performance of a system for automated detection of retinopathy in fundus images. The system was constructed entirely from published algorithms and it was tested in a large, representative, screening population. They achieved a sensitivity of 84% and a specificity of 64%. Assessed the efficacy of automated "disease/no disease" grading for retinopathy within a systematic screening programmer. Detection of retinopathy was achieved by automated grading with 90.5% sensitivity and 67.4% specificity [75]. The system designed by detected the fovea [76], blood vessel network, optic disk, as well as bright and dark lesions associated with retinopathy. They reported to have achieved classification accuracy of 90%. In area of the exudates, blood vessels and texture parameters coupled with neural network are employed to classify the retinal image into normal [77], NPDR and PDR. They reported a detection accuracy of 90% sensitivity [78]. Presented a computer based system for the identification of CSME, Non-CSME and normal fundus eye images. Here, features were extracted from the raw fundus images which are then fed to a neural network classifier to get the result. In [79] an automatic computerized screening system was developed to recognize automatically the main components of the retina. Diseased and normal retina was classified using multilayer perceptron neural network. Their system yielded a sensitivity of 80.21% and

70.66% specificity. In this work, a computer based system for automatic detection and grading of diabetic maculopathy severity level without manual intervention is presented. The optic disc is detected automatically and its location and diameter is used to detect fovea and to mark the macular region respectively. Next, hard exudates are detected using clustering and mathematical morphological techniques. Based on the location of exudates in marked macular region the severity level of maculopathy is classified into mild, moderate and severe. The method achieves a sensitivity and specificity of 95.6% and 96.15% with 130 retinal images for detecting maculopathy stages in fundus images as comparable to that of human expert. A graphical user interface has also been developed that can be used by clinicians during the mass screening of diabetic related eye diseases.

2.6 Summary

In this Chapter an insight into the domain knowledge, comprising of anatomy of the ocular fundus and the landmark retinal components were discussed. Two complications of diabetes, i.e., diabetic retinopathy and maculopathy were also discussed. This Chapter also provided a detailed literature on automatic detection of retinal anatomical, pathological structures and image analysis systems. From both number and diversity of algorithms used for retinopathy detection it is clear that there is no gold standard which solves the entire problem. Automated diabetic retinopathy detection system must serve patients in clinical practice. If it turns out that the reported approaches do not perform well in practical environments then we have to look for more theory so that we can design systems which cope better with the practical task. The discussion of this Chapter has led to the motivation for the development of fast automatic diabetic retinopathy screening system. The next four chapters propose the methods that lead to the development of this system capable of detecting the normal and abnormal features that aid ophthalmologists in diagnosing the severity stage of diabetic maculopathy

Chapter 3

Image Database and Preprocessing

Two publicly available retinal databases called DRIVE and STARE are used for testing the retinal vessel segmentation method and DIARETDB1 standard database is used for testing exudate detection method. The details of these databases are as follows.

The STARE Database: There are twenty retinal fundus slides and their ground truth images in the STARE (Structured Analysis of Retina) database. The images are digitized slides captured by a Top Con TRV-50 fundus camera with 35 degree field of view. Each slide was digitized to produce a 605 x 700 pixel image with 24- bits per pixel. All the twenty images were carefully labeled by hand to produce ground truth vessel segmentation by an expert. Figure 3.2 shows an example of an image from the database.

The DRIVE Database: The second image database is referred as the DRIVE (Digital Retinal Images for Vessel Extraction). The database consists of 40 color fundus photographs and their ground truth images.

All images in DRIVE database are digitized using a Cannon CR5 non- mydriatic 3CCD camera with a 45 degree field of view. Each image is captured using 24-bits per pixel at the image size of 565584. These images were labeled by hand, to produce ground truth vessel segmentation and Figure 3.3 shows one such image.

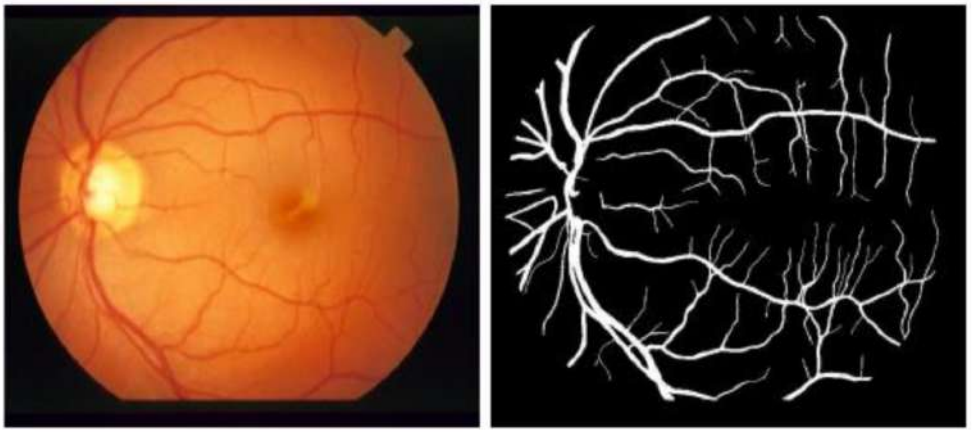

FIGURE 3.1: Retinal image from STARE database (left), hand labeled ground truth vessel segmentation (right)

DIARETDB1 Database: The database consists of 89 colour fundus images of which 84 contain at least mild non-proliferative signs of the diabetic retinopathy (see Figure 3.4), dand five are considered as normal which do not contain any signs of the diabetic retinopathy according to all the experts participated in the evaluation. Images were captured with the same 50 degree field-of-view digital fundus camera with varying imaging controlled by the system in the Kuopio university hospital, Finland. The image ground truth provided along with the database is based on expert selected findings related to the diabetic retinopathy and normal fundus structures. Special software was used to inspect the fundus images and annotate the findings as hard exudates, hemorrhages and microaneurysms.

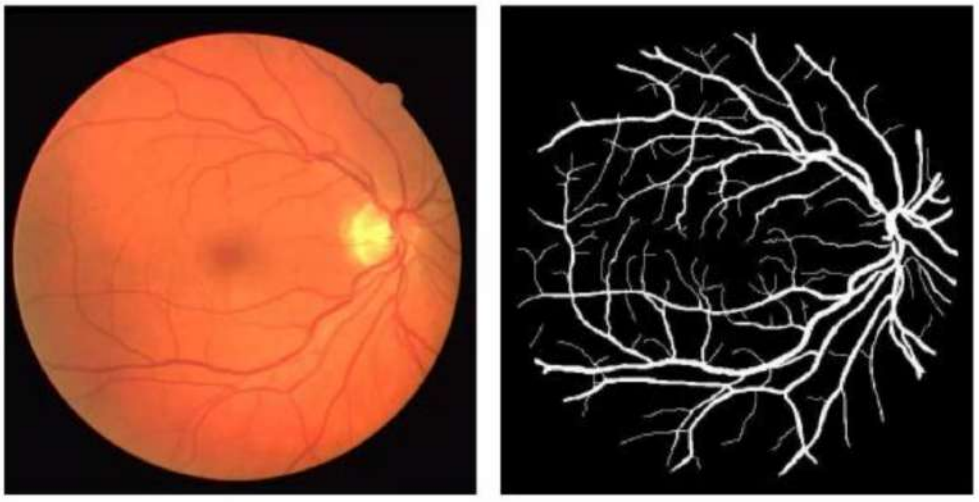

FIGURE 3.2: Retinal image from DRIVE database (left), hand labeled ground truth vessel segmentation (right).

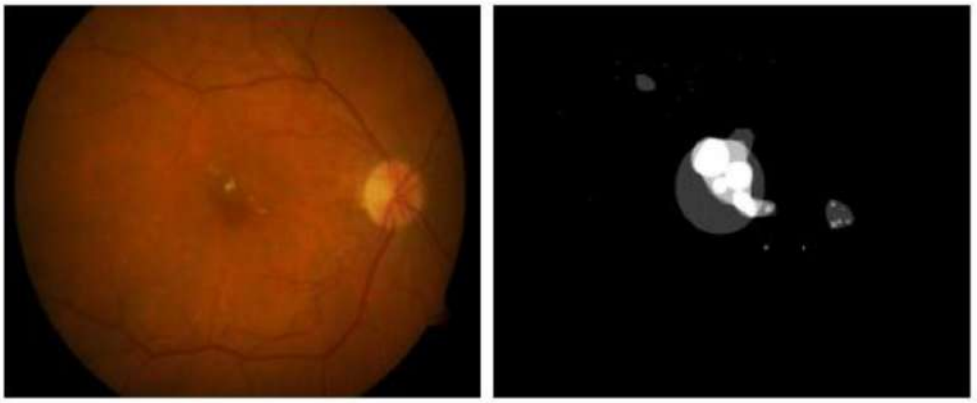

FIGURE 3.3: Example of abnormal fundus image from DIARETDB1 database (left), and Ground truth of hard exudates (right)

3.1 Preprocessing

Patient movement, poor focus, bad positioning, reflections, inadequate illumination can cause a significant proportion of images to be of such poor quality as to interfere with analysis. In approximately 10% of the retinal images, artifacts are significant enough to impede human grading. Preprocessing of such images can ensure adequate level of success in the automated abnormality detection. In the retinal images there can be variations caused by the factors including differences in cameras, illumination, acquisition angle and retinal pigmentation. First step in the preprocessing is to attenuate such image variations by normalizing the colour of the original retinal image against a reference image. Few of the retinal images acquired using standard clinical protocols often exhibit low contrast. Also, retinal images typically have a higher contrast in the centre of the image with reduced contrast moving outward from the centre. For such images, a local contrast enhancement method is applied as a second preprocessing step. Finally it is required to create a fundus mask for each image to facilitate segmentation of lesions and anatomical structures in later stages. The pre-processing steps are explained in detail in the following subsections.

3.1.1 Colour Normalization

Colour normalization is necessary due to the significant intra-image and inter- image variability in the colour of the retina in different patients. There can also be, differences in skin pigmentation, aging of the patient and iris colour between different patients

that affect the colour of the retinal image. Colour normalization method is applied to make the images invariant with respect to the background pigmentation variation between individuals. The colour normalization is performed using histogram matching [2]. In histogram matching a processed image can have a shape of the histogram as specified by the user. This is done by modifying the image values through a histogram transformation operator which maps a given initial intensity distribution into a desired distribution using the histogram equalization technique as an intermediate stage. Let Ps(s) and Pd(s) represent the standard image and desired image probability density functions, respectively. The histogram equalization of the standard image is as follows:

$$u = T(s) = \int_0^s p_s(x)dx \tag{3.1}$$

The histogram equalization of desired image is obtained by a similar transformation function as follows:

$$v = Q(d) = \int_0^d p_d(x)dx \tag{3.2}$$

The values of d for the desired image are obtained as follows:

$$d = Q^{-1}[u] = Q^{-1}[T(s)] \tag{3.3}$$

A standard retinal image is used as a reference for histogram specification technique in agreement with the expert ophthalmologist. This method is applied to normalize the values of only those images in the database that varies in colour with reference to the standard image. The histogram specification technique is independently applied to each individual RGB channel to match the shapes of three specific histograms of the reference image. Figure 3.5 (a) and (b) show the reference retinal image and its RGB histogram. To demonstrate the colour normalization effect, a different colour retinal image and its RGB histograms are shown in Figure 3.5 (c) and (d). The image normalized version and the relevant RGB histogram can be seen in Figure 3.5 (e) and (f). It can be seen that normalization process modifies the colour distributions of the considered image to match the reference image's distribution. This can be seen from comparison of the normalized image histograms with the reference image's histograms.

3.2 Diabetic Retinopathy

Diabetic retinopathy is a vascular disorder occurring due to the combination of micro-vascular leakage and micro-vascular occlusion within the retina [12]. It is primarily classified into Non-Proliferative Diabetic Retinopathy (NPDR) and Proliferative Diabetic Retinopathy (PDR). Typically there are no salient symptoms in the early stages of diabetic retinopathy, but the number and severity predominantly increase with the time. Non proliferative diabetic retinopathy is the most common and may arise at any point in time after the onset of diabetes. Ophthalmologists detect these changes by examining the patient's retina and look for spots of bleeding, lipid exudation, or areas of retinal swelling. Identification and recording of the following abnormalities (see Figure 1.3) will aid in the accurate assessment of retinopathy severity.

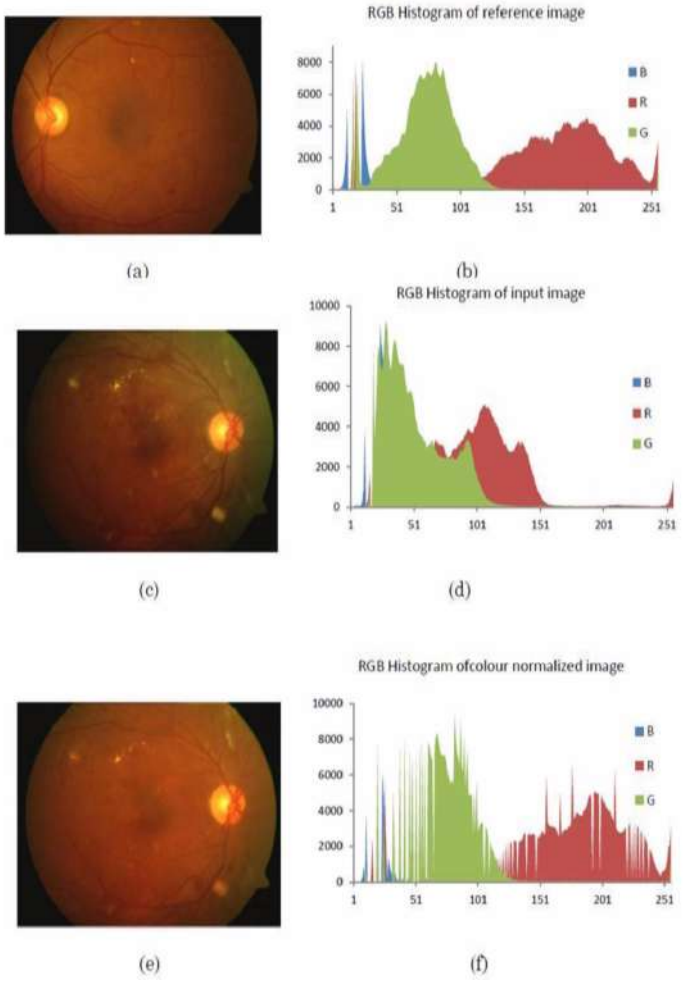

FIGURE 3.4: Colour normalization using histogram matching technique. (a) Reference colour retinal image; (b) RGB Histograms of reference image; (c) Input image; (d) RGB histograms of input image; (e) Colour normalized image; (f) RGB histogram of normalized image.

3.2.1 Contrast Enhancement

The contrast enhancement techniques are aimed at altering the visual appearance that makes an object distinguishable from other objects and the background. Usually retinal images acquired using standard clinical protocols often exhibit low contrast and may contain photographic artifacts. Also, it can be seen that retinal image contrast is decreased as the distance of a pixel from the centre of the image increases. In the current work this preprocessing step is applied to retinal images after the colour normalization.

At first, the red, green and blue space of the original image in Figure 3.6 (a) is transformed to Hue, Saturation and Intensity (HSI) space image. The HSI colour space is more appropriate for contrast enhancement as it allows the intensity to be treated separately from the other two components. Initially, on application of histogram equalization on the intensity image results in the image shown in Figure 3.6 (b). It can be seen that, even though the image quality is improved, the central part of the image and the optic disc region are both over-enhanced, which causes the image to lose important information. This is due to histogram equalization characteristic that treats the image globally. Since histogram equalization does not provide an efficient scheme, a Contrast-Limited Adaptive Histogram Equalization (CLAHE) technique is employed. While histogram equalization works on the entire image, CLAHE operates on small regions in the image, called tiles. Each tile's contrast is enhanced with histogram equalization. After performing the equalization, it combines neighbouring tiles using bilinear interpolation to eliminate artificially induced boundaries. While the contrast enhancement improves the contrast of exudate lesions it also enhances the contrast of some non- exudate background pixels, so that these pixels can wrongly be identified as exudate lesions. For this, a median filtering operation is applied on the intensity image prior to the contrast enhancement method to decrease this effect. Figure 3.6 (d) shows significant enhancement of contrast of the retinal image.

3.2.2 Fundus Mask Detection

The mask is a binary image with the same resolution as that of fundus image whose positive pixels correspond to the foreground area. It is important to separate the fundus from its background so that the further processing is only performed for the fundus and

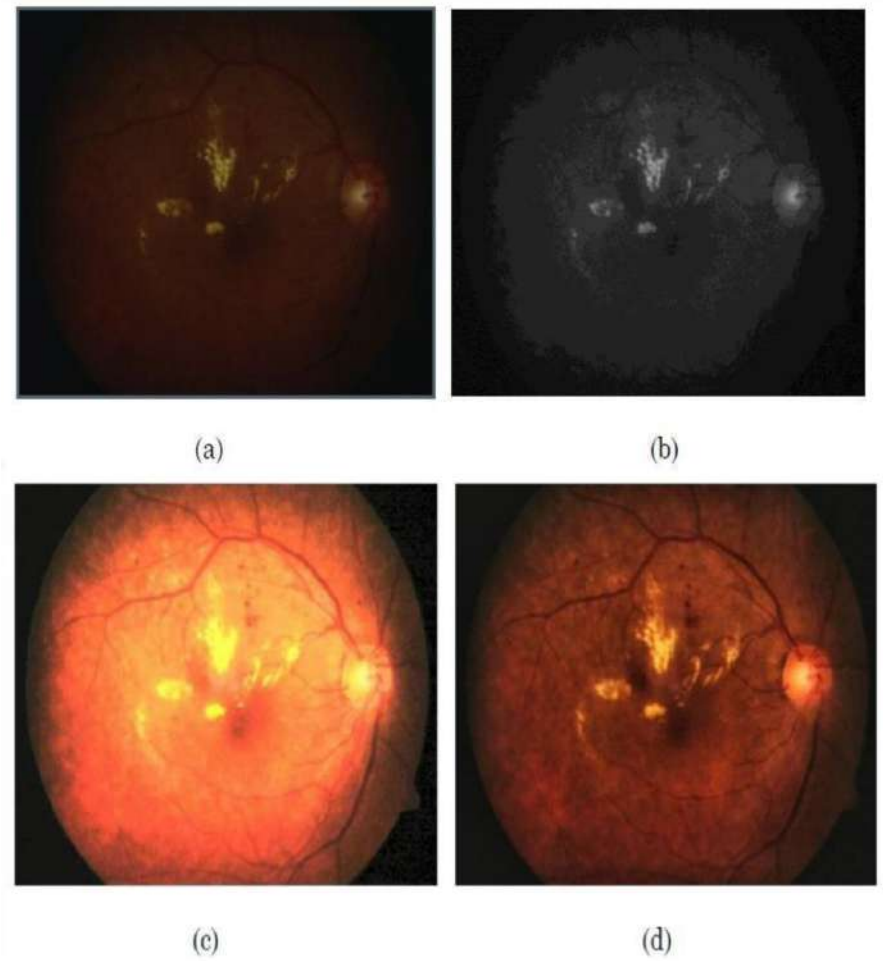

FIGURE 3.5: Contrast enhancement of retinal image using CLAHE technique. (a) Colour image before contrast enhancement; (b) Intensity image in HSI colour space; (c) Result of global histogram equalization; (d) Result of CLAHE

not interfered by pixels belonging to the background. In a fundus mask, pixels belonging to the fundus are marked with ones and the background of the fundus with zeros.

The fundus can be easily separated from the background by converting the original fundus image from the RGB to HSI colour system where a separate channel is used to represent the intensity values of the image. The intensity channel image is thresholded by a low threshold value as the background pixels are typically significantly darker than the fundus pixels. A median filter of size 55 is used to remove any noise from the created fundus mask and the edge pixels are removed by morphological erosion with a structuring element of size 55. Figure 3.7 (b) shows the example of the fundus mask.

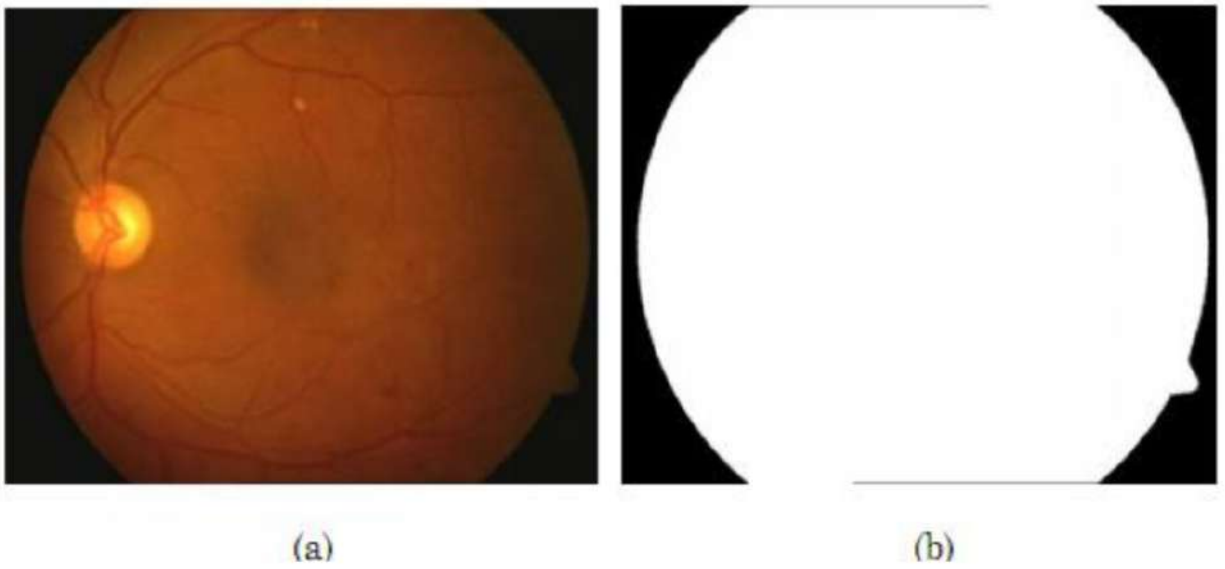

FIGURE 3.6: Automatic fundus masks generation. (a) Input image; (b) Automatically generated fundus mask

3.3 Summary

To develop an automatic retinal image processing system, the first important thing is to obtain an effective database. To realize this and also for facilitating comparison with the existing methods, four sets of Retinal databases are used. Details of the fundus camera and image properties of each of these databases are explained. In any retinal image database, there will be some images with non-uniform illumination and poor contrast. There can also be difference in the colour of the fundus due to retinal pigmentation among different patients. These images are preprocessed before they can be subjected to anatomical and pathological structure detection. Colour normalization is performed to attenuate colour variations in the image by normalizing the colour of the original retinal image against a reference image. In order to correct non-uniform illumination and to improve contrast of an image, contrast-limited adaptive histogram equalization is employed. On application of this method, the image quality is significantly improved with the increase in contrast. Each fundus camera has a mask of different shape and size according to its settings. By automatically detecting the fundus mask a lesion detection algorithm or vessel detection algorithm can process only the pixels of the fundus leaving out the background pixels. The following Chapters will explain the methods used to detect anatomical and pathological structures in retinal image leading

to the development of automatic system for the identification of severity levels in diabetic maculopathy.

Chapter 4

Automatic Segmentation of Retinal Vasculature

The segmentation and analysis of retinal vasculature form an essential part of several practical applications such as detection of hypertension, diabetes, stroke and cardiovascular diseases. In case of ophthalmologic conditions, the segmentation and measurement of the retinal vessels is of primary interest in the diagnosis and treatment of a diabetic retinopathy that directly affect the morphology of the retinal vessel tree. Also the accurate segmentation of the retinal blood vessels is often an essential prerequisite step in the automated analysis of retina for characterizing the detected lesions and in identifying false positives. For example, the performance of automatic detection of pathologies like microaneurysms and hemorrhages can be improved if regions containing vasculature are excluded from the analysis. In addition, the segmentation of the vessels is useful for image registration or spatial alignment of images. The registration of images, which are often acquired using different modalities, is useful for change detection, mosaic syn Dissertation and as a reference during laser treatment.

In ophthalmic imaging, the current standard used for acquiring the retinal image with enhanced blood vessels is through angiography using fluorescent dyes as shown in Figure 4.1. It requires the injection of a small amount of fluorescent dye into the patient, usually sodium fluorescein. Fluorescence angiography permits recording of blood vessels, flow and also the detection of leakages for diagnostic purposes.

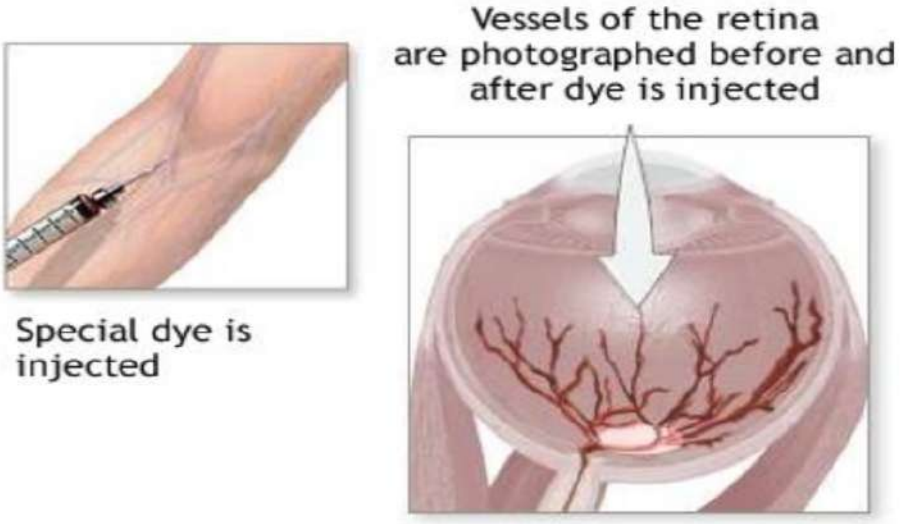

FIGURE 4.1: Fluorescein angiographic retinal image

However, this technique is not feasible during the mass screening of diabetic retinopathy as angiograms can only be obtained by specialists in ophthalmology clinics. Since the procedure is invasive, it often involves certain risk of side effects to the patient. Due to these limitations the need arises for segmentation of retinal vasculature from non-invasive colour fundus images. The properties and development of pixel level segmentation of retinal vessels without manual intervention is explained in the following sections.

4.1 Properties of Vessels

The retinal vasculature is mainly comprised of arteries and veins that are visible within the retinal image. These two spread out from the optic disc and branch successively to occupy different regions of the fundus. Compared to the other anatomical structures vessels have a lower reflectance. Thus, they appear darker relative to the background in the colour retinal image as shown in the Figure 4.2. Typically in a colour image with RGB channels, the red channel is oversaturated and the blue channel contains almost no information, while the bulk of the relevant data is contained within the green channel, as the following images show. Therefore, the blood vessels appear most contrasted in the green channel and it is used for automatic segmentation of vessels.

It was who proposed that vessels can be defined by a pair of parallel borders in such a manner that the shape of vessel cross-sections can be locally approximated by Gaussian functions [9]. Figure 4.3 shows one such gray-level profile of the cross section of small

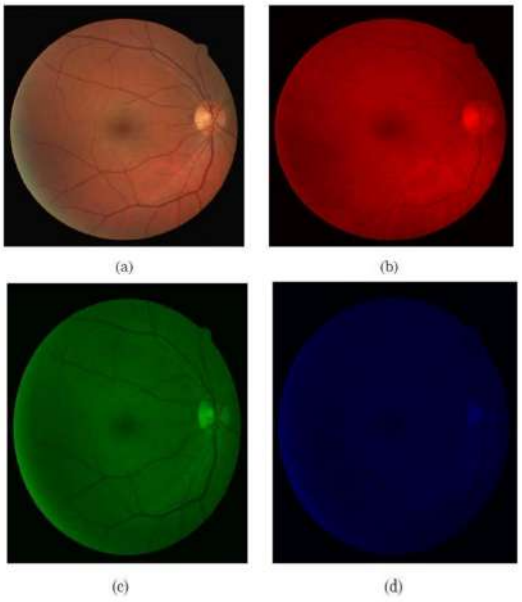

FIGURE 4.2: Appearance of vessels in different colour channels. (a) Colour retinal image; (b) Red channel image; (c) Green channel image; (d) Blue channel image

part of vessel. It clearly illustrates that whenever the line passes through the vessel, it forms a Gaussian shaped curve.

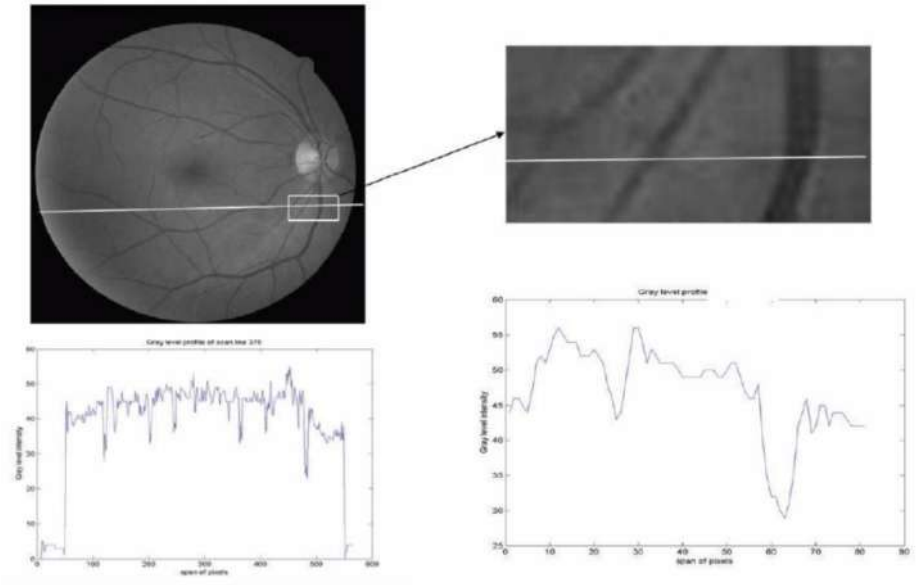

FIGURE 4.3: Gray level profile of cross section of blood vessel

The vessels usually have a limited curvature and are often approximated by piecewise linear segments. Even though the width of the vessels decreases as they move radially outward from the optic disc, the change is gradual one. The widths of the vessels are found to lie within a range of 40-200 m in a standard retinal image. These properties were exploited and a matched filter was designed to segment the vessels. But the

matched filter provides poor spectral response because of the background variation and low contrast of the smaller vessels. It also increases the number of false responses around bright objects and reflection artifacts. Therefore, a high quality filter capable of handling all these constraints is to be provided. A set of Gabor filters tuned to particular frequency and orientation offers a better solution than the matched filters.

4.2 Vessel Enhancement Using 2-D Gabor Filters

The Gabor filters are sinusoid ally modulated Gaussian functions that have optimal localization in both the frequency and space domains [80]. They have been extensively used within the computer vision community, with special attention to its relevance to studies of the human visual system [81]. Gabor filters have been widely applied to image processing application problems such as texture detection and segmentation, motion estimation, object detection, strokes in character recognition and roads in satellite image analysis [82]. The three major properties of the Gabor filter includes: Ability to be tuned to specific orientations. This allows the extraction of the features of line segment at any possible orientation [83]. Second, the bandwidth of the filter is adjustable. Finally the output of the filter is robust to noise as it uses information of all the pixels within the kernel [84]. The real part of 2D Gabor filter used in the context of retinal vessel segmentation is defined in the spatial domain $g(x, y)$ as follows:

$$g(x,y) = exp\left[-\pi\left(\frac{x_p^2}{\sigma_x} + \frac{y_p^2}{\sigma_y}\right)\right]\cos\left(2\pi f x_p\right) \tag{4.1}$$

Where,

$$x_p = x\,cos\theta + y\,sin\theta$$

$$y_p = -x\,sin\theta + y\,cos\theta$$

The parameters present in the Gabor function defined above are as follows [85]. The angle is orientation of the filter, for example, an angle of zero gives a filter that responds well to the vertical features in an image [83]. The parameter is the central frequency of pass band. Next, is the standard deviation of gaussian in x direction along the filter that determines the bandwidth of the filter finally, is the standard deviation of gaussian across the filter that controls the orientation selectivity of the filter?

4.2.1 Estimation of Gabor Parameters

The size and shape of the lines or curvilinear structures to be detected are to be considered for deriving the Gabor parameters. In the case of vessel segmentation, the Gabor filter should be tuned to a suitable frequency, so that vessels may be emphasized while background noise and other undesirable structures are filtered out. In the procedure to obtain the Gabor parameter values for the detection of straight line with width t has been described. The same procedure is used to estimate the Gabor parameters to detect vessels oriented in different directions. The frequency f= determines the 2D spectral centroid positions of the Gabor filter

The standard deviation σ_x determines the spread of the Gabor filter in the θ direction and it is given by $\sigma_x = \lambda t/0.75\pi$. The standard deviation σ_y that specifies the elongation of the filter is given by $\sigma_y = 0.85\sigma_x$,where $\lambda = \sqrt{2\ln 2/\pi}$.

This parameter is derived with respect to the average width of the piecewise linear segments of retinal vessels and it is set to With the parameters set, the Gabor filter is thus said to be directional, as its spatial domain support is an ellipse given by the elongated gaussian of equation 4.1. Since, blood vessels have varying diameters along different branches, appropriate value of the thickness t has to be set. When the value of t is large, most small vessels are depressed by neighbouring noise. In manual segmentation it is found that majority of the vessel diameters are of 120 m wide in a standard fundus image with resolution of 20micron/pixel. Therefore to accommodate all vessels in the image, thickness parameter t is set to six for enhancing and preserving of small vessels as well. The surface representation and real part of resulting Gabor kernel is shown in Figure 4.4 with angle set to zero. It can be seen that it is suited for the orientation of directional features to provide good response for pixels associated with retinal blood vessels. It can be noted that the shape of the Gabor is locally similar to that of a blood vessel and is preserved across different orientations. Therefore, stronger Gabor responses are produced when the filter is found at the same position, orientation and scale as a vessel in the image.

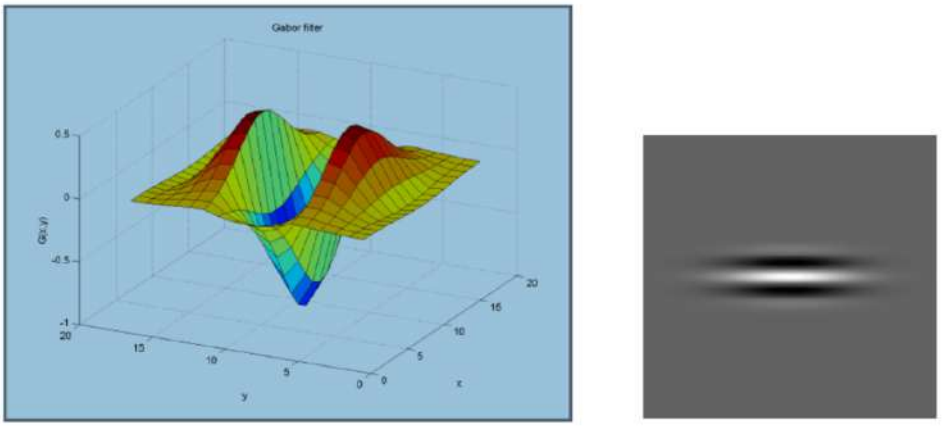

(a) (b)

FIGURE 4.4: Gabor filter; (a) Surface representation; (b) Real part of filter

4.2.2 Spatial Filtering of Vessels

Spatial filtering is performed on the input retinal image to highlight the vessel structures while suppressing the background noise and other artifacts. As mentioned earlier, the green channel in the RGB image provides the best vessel to background contrast, than the red and blue channels. Therefore, only the green channel image is used for further processing in the vessel segmentation method. Because of the directional selectivity of the Gabor filter, it is possible to enhance pixels of vessels oriented along various directions with the parameters as described earlier. The response of applying a Gabor filter to a vessel segment is given by

$$r(x,y) = g(x,y) * I_g(x,y) \tag{4.2}$$

Where, $g(x,y)$ is the Gabor filter defined by equation 4.1 and $Ig(x,y)$ is a green channel image with vessel segment oriented along different directions. It can be seen that the shape of the filter similar to the vessels and when it is positioned at the center of a vessel at scale and orientation, it provides maximum response along the vessel direction and minimum responses along its perpendicular direction. In order to detect the vessels oriented along different directions, the filter has to be rotated along those directions and only maximum response at that position is retained as follows.

$$r_{max}(x,y) = \max_{\theta}[r(x,y)] \tag{4.3}$$

For each pixel position in an image, spatial filtering is performed by convolving image with the Gabor kernel along different orientations. It is also found in the literature that vessel segments lying within 7.5 degree of direction of chosen kernel will respond well. So the angle of Filter is rotated from 0 to 170 degrees in steps of 15o to produce a single peak response on the center of a vessel segment. Figure 4.5 shows the response of vessels for a filter with orientation along 0 o, 45o and 90o. It can be seen that only the vessels along that direction respond maximum than vessels oriented in different direction.

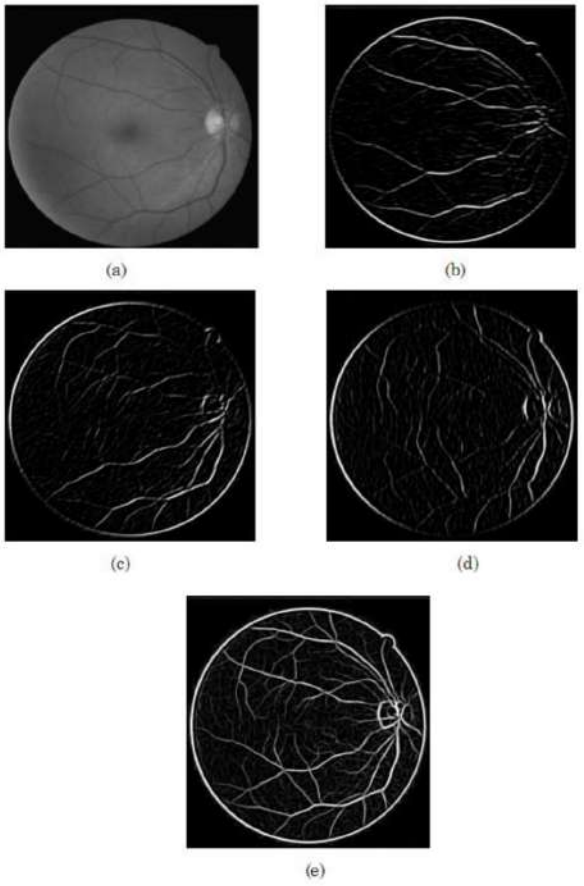

FIGURE 4.5: Gabor Filter Response (GFR) images; (a) Input image; (b) GFR for = 00; (c) GFR for = 450; (d) GFR for = 900; (e) Overall Gabor response image with enhances vessels.

4.2.3 Segmentation of Vessels

When the retinal vessels have been enhanced compared to the background, the next step is to extract the vessels from the image. In order to properly extract the enhanced vessel segments in the Gabor filter response image, an effective thresholding scheme is required. The entropy based thresholding using gray level co-occurrence matrix is

employed. It computes optimal threshold by taking into account the spatial distribution of gray levels that are embedded in the co- occurrence matrix. From the co-occurrence matrix, several types of entropies such as global, local, joint and relative entropy can be computed to determine the threshold value [7]. This technique is simple and easy to use because the co- occurrence matrix contains most information needed for threshold value computation. For the proper segmentation of vessel pixels, a threshold is calculated using local entropy. The following section gives the computation of threshold in detail.

4.2.4 Gray Level Co-occurrence Matrix

The GLCM contains information on the distribution of gray level frequency and edge information, as it is very useful in finding the threshold value [86]. The gray level co-occurrence matrix is a LL square matrix of the gray scale image I of spatial dimension MN with gray levels in the range [0, 1. . . L-1]. It is denoted by T = [ti, j]LL matrix. The elements of the matrix specify the number of transitions between all pairs of gray levels in a particular way [87]. For each image pixel at spatial co-ordinate (m, n) with its gray level specified by f(m ,n), it considers its nearest four neighbouring pixels at locations of (m+1, n), (m-1, n), (m, n + 1) and (m, n - 1). The co-occurrence matrix is formed by comparing gray level changes of f(m, n) to its corresponding gray levels, f(m +1, n), f(m -1, n), f(m, n + 1) and f(m, n - 1). Depending upon the ways in which the gray level i follows gray level j, different definitions of co-occurrence matrix are possible. The co-occurrence matrix by considering horizontally right and vertically lower transitions is given by

The spatial co-occurrence matrix thus obtained from the gray level Gabor response image is shown in the Figure 4.6.

4.2.5 Entropic Thresholding

Based on the gray level variation within or between object and background, the gray level co-occurrence matrix is divided into quadrants. Let Th be the threshold within the range $0ThL-1$, that partitions the gray level co-occurrence matrix into four quadrants, namely A, B, C and D.

$$t_{i,j} = \sum_{m=1}^{M} \sum_{n=1}^{N} \delta \tag{4.4}$$

where

$$\delta = 1 \quad if \begin{cases} f(m,n) = i \; and \; f(m,n+1) = j \\ or \\ f(m,n) = i \; and \; f(m+1,n) = j \end{cases}$$

$$\delta = 0 \quad otherwise$$

Normalizing the total number of transitions in the co-occurrence matrix, a desired transition probability $P_{i,j}$ from gray level i to gray level j is obtained as follows.

$$P_{i,j} = \frac{t_{i,j}}{\sum_{i=1}^{L} \sum_{j=1}^{L} t_{i,j}} \tag{4.5}$$

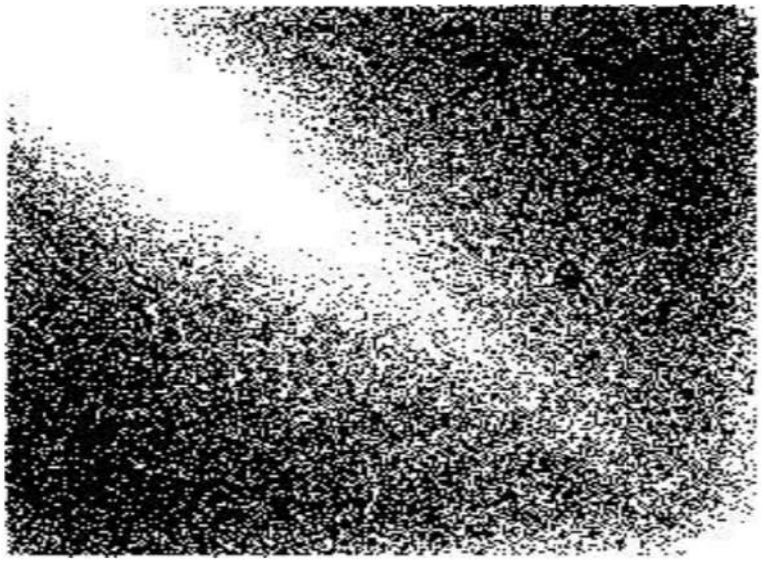

FIGURE 4.6: Gray level co-occurrence matrix

In the Figure 4.7, quadrant A represents gray level transition within the object while quadrant C represents gray level transition within the background. The gray level transition between the object and the background or across the object's boundary is placed in quadrant B and quadrant D. These four regions can be further grouped into two classes, referred to as local quadrant and joint quadrant. Local quadrant is referred to quadrant A and C as the gray level transition that arises within the object or the background of the image. Then quadrant B and D is referred as joint quadrant because the gray level transition occurs between the object and the background of the image. The local entropic threshold is calculated considering only quadrants A and C. The

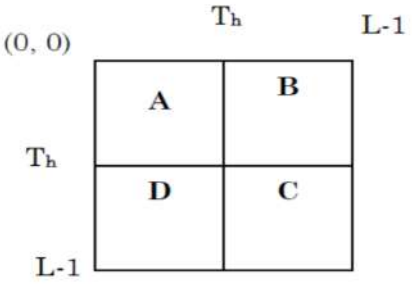

FIGURE 4.7: Four quadrants of co-occurrence matrix

probabilities of object class and background class are defined as

$$P_A = \sum_{i=0}^{T_h} \sum_{j=0}^{T_h} P_{i,j} \tag{4.6}$$

$$P_C = \sum_{i=T_h+1}^{L-1} \sum_{j=T_h+1}^{L-1} P_{i,j} \tag{4.7}$$

Using equations 4.6 and 4.7 as normalization factors, the normalized probabilities of the object class and background class are functions of threshold vector (Th, Th) are defined as

$$P_{i,j}^A = \frac{P_{i,j}}{P_A} \tag{4.8}$$

$$P_{i,j}^C = \frac{P_{i,j}}{P_C} \tag{4.9}$$

From these, the local transition entropy A denoted by Ha (Th) and C denoted by Hc (Th) are calculated as follows: The second-order entropy of the object is given by

$$H_A(T_h) = -\frac{1}{2} \sum_{i=0}^{T_h} \sum_{j=0}^{T_h} P_{i,j}^A log_2 P_{i,j}^A \tag{4.10}$$

Similarly, the second-order entropy of the background is given by

$$H_C(T_h) = -\frac{1}{2} \sum_{i=T_h+1}^{L-1} \sum_{j=T_h+1}^{L-1} P_{i,j}^C log_2 P_{i,j}^C \tag{4.11}$$

Both Ha (Th) and Hc (Th) are determined by threshold Th, thus they are functions of Th. By summing up the local transition entropies, the total second-order local entropy of the object and the background is given by

$$H_T(T_h) = H_A(T_h) + H_C(T_h) \qquad (4.12)$$

F inally, TE the gray level corresponding to the maximum of HT (Th) over Th gives the optimal threshold for value.

$$T_E = arg\left[\max_{T=0\ldots L-1} H_T(T_h)\right] \qquad (4.13)$$

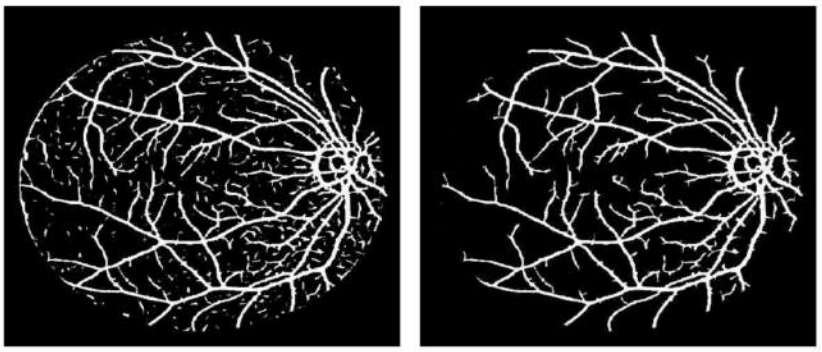

FIGURE 4.8: Segmented vessels; (a) Threshold Gabor response image; (b) Final segmented image after removing unconnected pixels

Figure 4.8 shows the application of the threshold to the Gabor response image in Figure4.5. It can be seen that there exists small unconnected pixels in the thresholded image. These isolated pixels are removed by performing length filtering based on connected pixel labeling. The result of removing these unconnected pixels can be seen in the final segmented image. To ensure that only the section of the image containing data is considered during image processing and analysis, a mask image is generated for each image as described in the Chapter 3 of the Dissertation. It is applied to remove any artifacts present outside the region of interest.

4.3 Results and Discussion

The retinal images from the DRIVE database and STARE database are used for evaluating the performance of the vessel segmentation method. The manually segmented vessels provided in both the databases are used as gold standard. Figure 4.9 and Figure 4.10 illustrates the result of vessel segmentation on one of the images in each database. The entire process of segmenting vessels was performed on Intel PC with 1.66 GHz CPU

and 512MB memory using Matlab9 Matlab12. The processing of each image including convolution and thresholding took about 30 seconds.

Bank of twelve Gabor filters oriented in the range of 0 to 170 degrees are used to enhance the multi-oriented vessels. Increasing the number of filter banks did not result in significant improvement of result but increased the convolution operations. For each of the images a corresponding manually segmented image is provided. It is binary image with pixels that are determined to be part of a blood vessel by a human observer under the instruction of an ophthalmologist are coloured white. Quantitative evaluation of the segmentation algorithm is done by comparing the output image with the corresponding manually segmented image. The comparison yields statistical measures that can be summarized using contingency table, as shown in Table 4.1. True positives are pixels marked as vessel in both the segmentation given by a method and the manual segmentation used as ground truth. False positives are pixels marked as vessel by the method, but that are actually negatives in the ground truth. True negatives are pixels marked as background in both images. And false negatives are pixels marked as background by the method, but actually are vessel pixels.

TABLE 4.1: Performance analysis

	GROUND TRUTH		
		Positive	Negative
Method Result	Positive	True Positive(Tp)	False Positive(Fp)
	Positive	True Negative(Tn)	Negative(Fn)

From these sensitivity and specificity are evaluated. Sensitivity gives the percentage of pixels correctly classified as vessels by the method and specificity gives the percentage of non-vessels pixels classified as non-vessels by the method as follows,

$$Sensitivity = \frac{T_p}{T_p + F_n} \tag{4.14}$$

$$Specificity = \frac{T_n}{T_n + F_p} \tag{4.15}$$

Where Tp is true positive, Tn is true negative, Fp is false positive and Fn is false negative at each pixel. The method is compared with the matched filter based method of using the DRIVE database. Table 4.2 shows that Gabor filter is better in classifications of vessels with less false positive fraction rate.

TABLE 4.2: Performance of retinal blood vessels segmentation method on DRIVE Database

Method	Sensitivity (%) Mean SD	Specificity (%) Mean SD
Gabor filter based	86.47 3.6	96 1.01
Matched filter based	83.79 2.62	89.59 3.83

The methods are also evaluated using receiver operating characteristic (ROC) curve. ROC curves are formed by ordered pairs of true positive (sensitivity) and false positive (1-specificity) rates. The points on the ROC curve are obtained by varying the threshold on the Gabor filter output image. For each configuration of threshold value, a pair formed by a true positive and false positive rate corresponding to the method's output is marked on the graph, producing a curve as in Figure 4.11. The closer an ROC curve is to the upper left corner, the better the method's performance, with the point (0,1) representing a perfect agreement with the ground truth. Accordingly, an ROC curve is said to dominate another if it is completely above and to the left of it. In the experiment performed, the optimal threshold used to get the final output is varied in steps of 5 to get number of points on the ROC curve for both the methods. In the Figure 4.9 it can be clearly visualized that the Gabor filter method performs better to that of matched filtered based method.

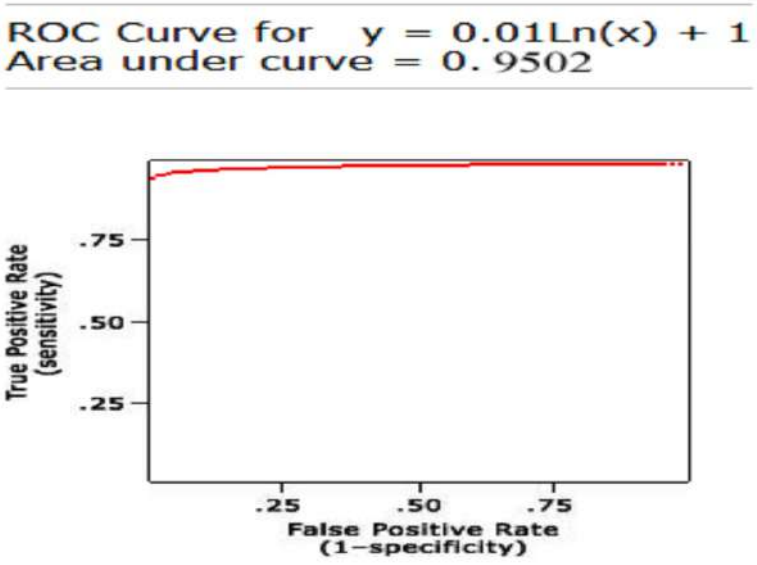

FIGURE 4.9: ROC curves of Gabor and Matched filter methods

The results of the proposed method are also compared with those [88] of on twenty images from the STARE database and the result is depicted in Table 4.3. Here also the

TABLE 4.3: Comparison of vessel segmentation results on STARE database

Method	Sensitivity (%)	Specificity (%)
Proposed method	85	96
Hoover [88]	75	92

proposed method performs better with lower specificity even in the presence of lesions in the abnormal images.

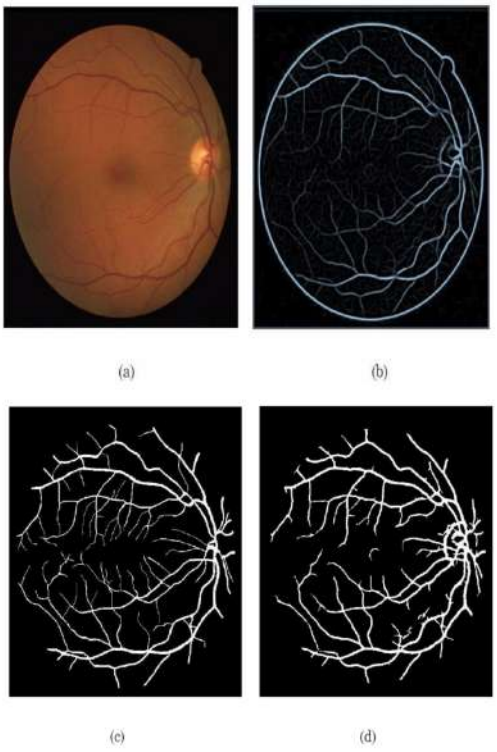

FIGURE 4.10: Result of vessel segmentation on image from DRIVE database; (a) Input image; (b) Gabor response image; (c) Manual segmentation by expert; (d) Automatic Segmentation by the method.

Apart from two standard databases the method is also tested on retinal images obtained from Ophthalmology department. These images are of large variability in terms of presence of lesions and image quality. These are considered to evaluate the robustness of the method. The result for one of the image is shown in Figure 4.12 and is validated by ophthalmologists.

4.4 Summary

An efficient method for automatic segmentation of retinal blood vessels has been presented in this Chapter. Colour retinal images from three different databases were used

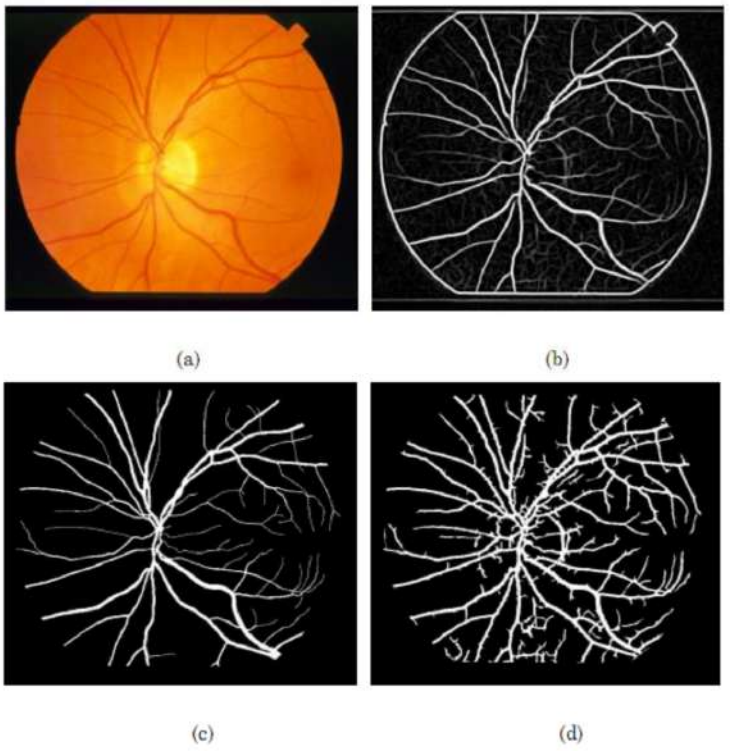

FIGURE 4.11: Result of vessel segmentation on image from STARE database; (a) Input image; (b) Gabor response image; (c) Manual segmentation by expert; (d) Automatic Segmentation by the method

FIGURE 4.12: Vessel segmentation result on image from DIARETDB0 database

to evaluate the robustness and accuracy of the method. Based on the results obtained it can be demonstrated that the method will be useful in a wide range of retinal images. A brief comparison with some other vessel segmentation algorithms was also provided. It can be concluded that the Gabor filter provides better results when compared with other filter based methods. Since the scale of the Gabor filter can be changed, it will be very useful in multi-scale analysis of vessels. For the pixel level classification of vessels entropic threshold provides a fast and better result. The segmented vessels can be used to obtain the control points used in the retinal registration techniques. Based on the tortuosity of segmented vessels it is possible to quantify the proliferative diabetic retinopathy. It is hoped that vessel segmentation aids clinicians to detect and monitor the progression of disease, minimize the examination time and helps in the better treatment plan.

Chapter 5

Detection of Optic Disc and Macula

An efficient detection of optic disc in colour retinal images is a significant task in an automated retinal image analysis system. Its detection is prerequisite for the segmentation of other normal and pathological features. For i n s t a n c e , the measurement of varying optic disc to cup diameter ratio is used in the detection sight threatening disease called glaucoma. The position of optic disc can be used as a reference length for measuring distances in retinal images, especially for the location of macula. In case of blood vessel tracking algorithms the location of optic disc becomes the starting point for vessel tracking. It also acts as landmark feature in registration of multimodal or temporal images. Finally, in case of diabetic maculopathy lesions identification, masking the false positive optic disc region leads to improvement in the performance of lesion detection. The attributes of optic disc is similar to attributes of hard exudates in terms of colour and brightness. Therefore it is located and removed during the hard exudates detection process, thereby avoiding false positives. In colour fundus photograph shown in Figure 5.1 optic disc appears as a bright spot of circular or elliptical shape, interrupted By the outgoing vessels. It can be seen that optic nerves and vessels emerge into the retina through optic disc. It is situated on the nasal side of the macula and it does not contain any photoreceptor. Therefore it is also called the blind spot.

The size of optic disc varies from patient to patient, but its diameter always lies between 80 and 100 pixels in a standard fundus images. There are many factors that make

accurate optic disc boundary detection a difficult task. In most of the images the disc boundaries are not clearly visible. And also, several parts of disc will be obscured by the crossing blood vessels. In the current work, the segmentation of optic disc boundary is performed in two steps. First the disc is spatially localized and its approximate center is determined using iterative thresholding and connected component method. This provides a baseline for finding of its exact boundaries. Then, the geometric model based implicit active contour is employed to obtain accurate optic disc boundary. The method was tested on 130 images and qualitatively evaluated by comparing the automatically segmented disc boundaries with manual ones drawn by an experienced ophthalmologist. The details of the optic disc localization and boundary detection methods are described in the following sections.

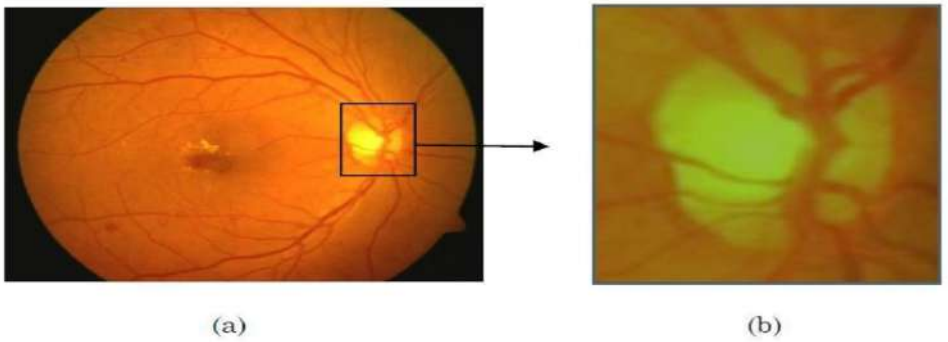

FIGURE 5.1: Colour retinal image; (a) Optic disc location in the retinal image (b) Enlarged optic disc area

5.1 Localization of Optic Disc

The localization of optic disc is important for two purposes. First, it serves as the baseline for finding the exact boundary of the disc. Secondly, optic disc center and diameter are used to locate the macula in the image. In a colour retinal image the optic disc belongs to the brighter parts along with some lesions. The central portion of disc is the brightest region called optic cup, where the blood vessels and nerve fibers are absent. Applying a threshold will separate part of the optic disc and some other unconnected bright regions from the background. In this work an optimal thresholding based on method is applied to separate brighter regions from dark background as follows.

5.1.1 Selection of Initial Threshold

Optimal thresholding method based on approximation of the histogram of an image using a weighted sum of two or more probability densities with normal distribution is used for initial thresholding of the retinal image. Histogram information derived from the source image is used to partition the brightest regions from background. It is observed that disc appears most contrasted in the green channel compared to red and blue channels in the RGB image. Therefore, only the green channel image is used for calculating the optimal threshold. Figure 5.2 shows the input green channel image and its histogram. It can be seen that the pixels corresponding to the optic disc and the optic cup belong to the higher intensity bars in the histogram. The diameter of the optic disc is in the range of 1.8 to 2mm. Based on the visual inference in a standard retinal image with 768576 size with 20micron/pixel resolution, this prior information is used to calculate the threshold.

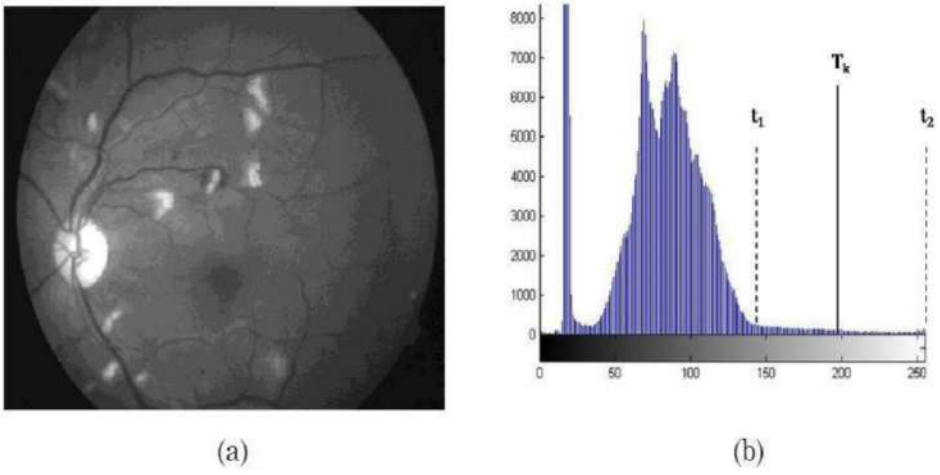

FIGURE 5.2: Selecting an optimal threshold; (a) Gray scale of green channel retinal image; (b) Corresponding histogram with initial threshold

To obtain an optimal threshold, histogram derived from the source image I is scanned from highest intensity value l2 to lower intensity value. The scanning stops at the intensity level l1 which has at least a thousand pixels with the same intensity. The initial threshold Tk for step k=1 is taken as the mean of t2 and t1 resulting in subset of histograms. Formulation for the calculation of optimal threshold is given by the following pseudo code.

- Initial estimate of Tk is calculated at step k as

$$T_k = \frac{l_1 + l_2}{2} \tag{5.1}$$

- At step k, apply the threshold. Tk this will produce two groups of pixels: Go consisting of all pixels belonging to object region and Gb consisting of all pixels belonging to background region.
- Compute the average intensity values U^k and U^k for the pixels in Go and Gb respectively.
- Update the threshold as follows:

$$T_{k+1} = \frac{\mu_o^k + \mu_b^k}{2} \tag{5.2}$$

- Repeat steps 2 through 4 differences in T in successive iterations is smaller than a predefined value.

Optimal threshold thus calculated results in maximization of gray level variance between object and background. Figure 5.3 shows the result of thresholding on one of the test image resulting in number of isolated connected regions.

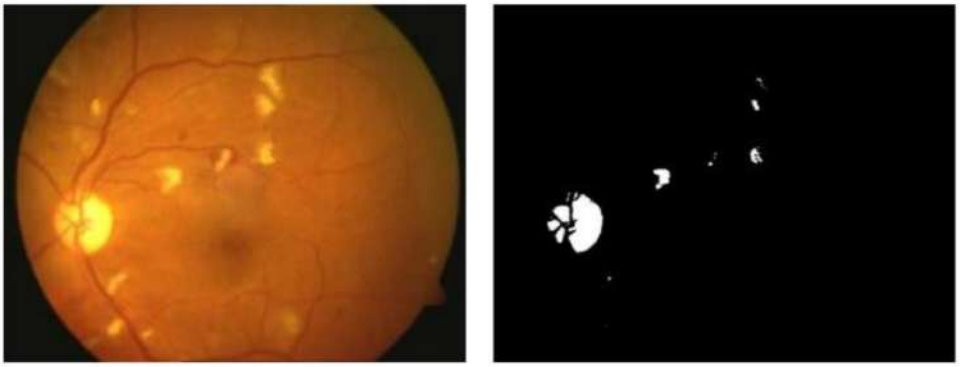

(a) (b)

FIGURE 5.3: Optimal thresholding of retinal image; (a) Input colour retinal image; (b) Thresholded image with number of connected regions

5.1.1.1 Estimation of the Optic Disc Center

Thresholding of an image results in number of connected components such as part of optic disc, some noise and other bright features. These connected components are candidate regions for optic disc. The entire image is scanned to count the number of connected components. Each of the connected components in the thresholded image is labeled, total number of pixels in the component and mean spatial coordinates of each connected component is calculated. The component having the maximum number of pixels is assumed to be having the optic cup part of disc and it is considered to be the primary region of interest. The maximum diameter of optic disc can be of 2mm. Therefore, in an image, if any of the components whose mean spatial coordinates are within 50 pixels distance from the mean spatial coordinates of the largest component, then they are merged with it and new mean spatial coordinate is calculated. Figure 5.4 illustrates the merging of components if they are part of optic disc.

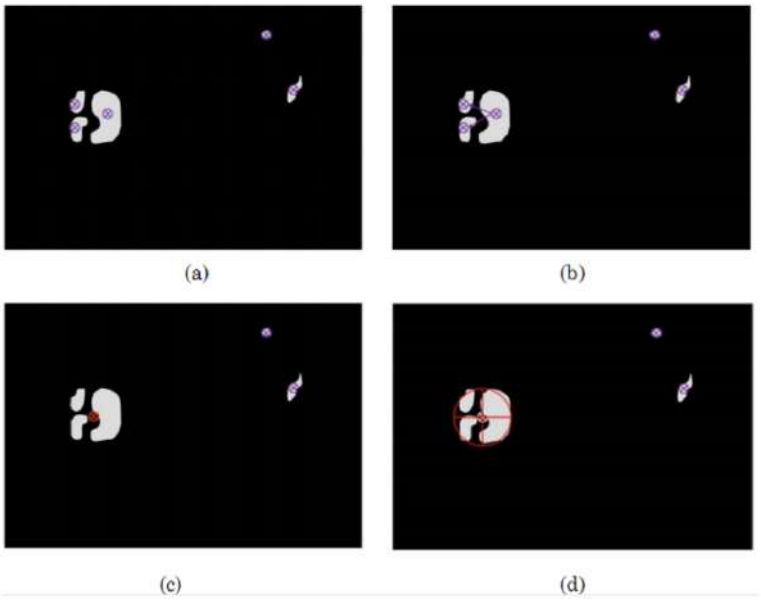

FIGURE 5.4: OEstimating center of optic disc; (a) Candidate regions; (b) Merging of the nearby components into largest component; (c) New centroid of merged region; (d) Ellipse drawn to show the located disc centered at centroid of disc.

If this region is equal to or greater than 1.8mm in diameter an ellipse is drawn to indicate the location of optic disc with its approximate center. Otherwise the threshold is decremented by one and applied to the initial image only in the local rectangular region within the vicinity of the mean spatial coordinates computed earlier. This is to

avoid misclassifying lesions as a part of the optic disc. The iterative process is repeated until an optimal size of the optic disc is obtained.

The following Figure 5.5 illustrates the optic disc localization through iterative process and its center estimation.

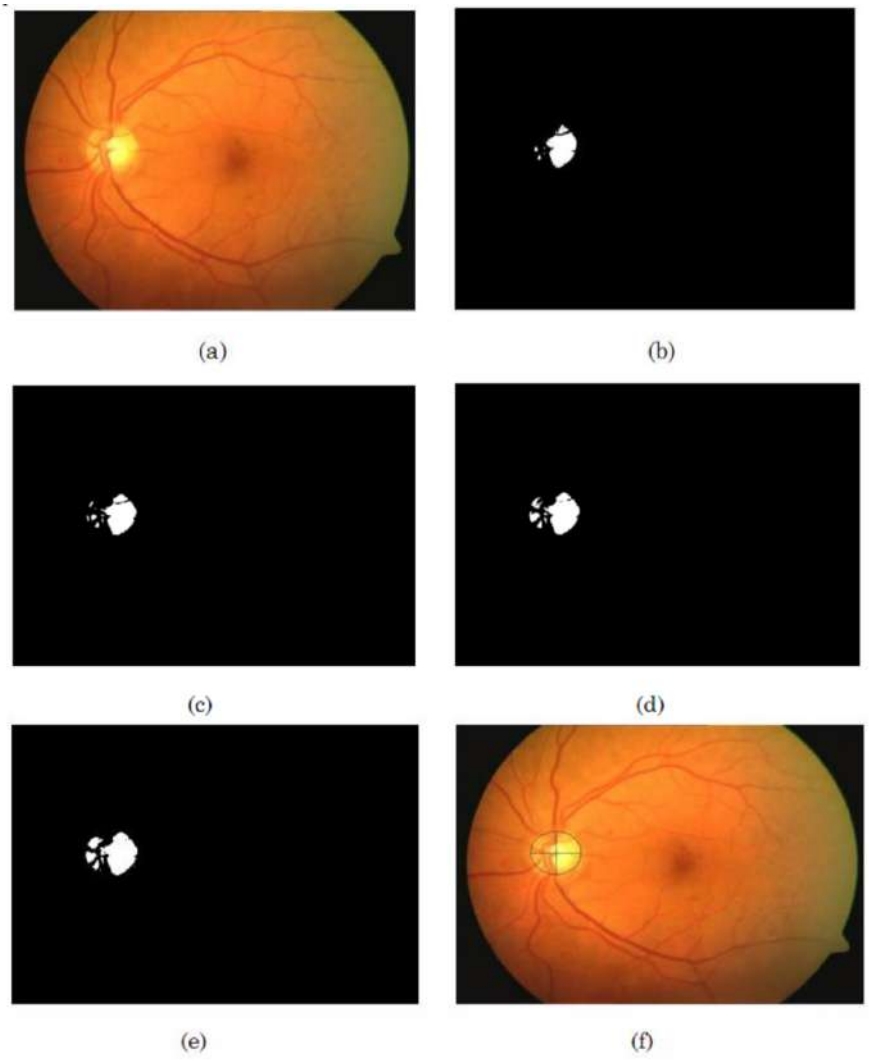

FIGURE 5.5: Localization of optic disc; (a) Input colour retinal image; (b) Initial thresholding; (c)-(e) Detection phase; (f) Ellipse drawn to show location of optic disc.

5.1.2 Optic Disc Boundary Detection

Glaucoma is the second most common cause of blindness worldwide [89]. It is characterized by elevated Intra Ocular Pressure (IOP), which leads to damage of optic nerve axons at the back of the eye, with eventual deterioration or loss of vision. Progression of glaucoma is slow and silent leading to changes in the shape and size of the optic disc.

Therefore, assessment of optic disc size is an important component of the diagnostic evaluation for glaucoma. This has led to the motivation for the accurate detection of optic disc boundary as it is used to detect and measure the severity of disease.

Difficulty in finding the optic disc boundary is due to its highly variable appearance in retinal images. Classical segmentation algorithms such as edge detection, thresholding, and region growing are not enough to accurately find boundary of the optic disc as they do not incorporate the edge smoothness and continuity properties. In contrast, active contour model represent the paradigm that the presence of an edge depends not only on the gradient at a specific point but also on the spatial distribution [90]. Active contours incorporate the global view of edge detection by assessing continuity and curvature, combined with the local edge strength thus providing smooth and closed contours as segmentation results. These properties make them highly suitable for the optic disc boundary detection application. Active contours are energy minimizing splines and are generally classified as parametric or geometric according to their representation. In the proposed work, the automatic optic disc boundary is detected by fitting an implicit active contour based on geometric model as reported in. Geometric based model differ from parametric models in the sense that they do not depend much on image gradient and are less sensitive to location of initial contour, thus performs better for object with weak boundaries as in case of optic disc. The following sections provide the details of optic disc boundary segmentation using geometric active contours.

5.1.2.1 Elimination of Vessels

The optic disc region is usually fragmented into multiple sub-regions by blood vessels that have comparable gradient values. A homogeneous optic disc region is needed for segmentation using geometric active contour algorithm. Use of median filter with appropriate size to remove interfering blood vessels from the optic disc region resulted in heavy blurring of disc boundaries. Instead a better result is achieved with gray level mathematical morphology to remove irrelevant vessels from the optic disc region.

Gray scale mathematical morphology provides a tool for extracting geometric information from gray scale images. A structuring element is used to build an image operator whose output depends on whether or not this element fits inside a given image. Shape and size of the structuring element is chosen in accordance with the segmentation task.

The two fundamental morphological operations are dilation and erosion. Denoting an image by I and structuring element by S, the Dilation and erosion at a particular pixel (x, y) are defined as:

$$(I \oplus S)(x,y) = \max_{i,j}[I(x-i, y-j) + S(i,j)] \quad (5.3)$$

$$(I \ominus S)(x,y) = \min_{i,j}[I(x+i, y+j) - S(i,j)] \quad (5.4)$$

Where and j index the pixels of S. The opening of an image is defined as erosion followed by dilation. It tends to smooth the small-scale bright structures in an image. The closing of an image is defined as dilation followed by erosion that tends to smooth the small-scale dark structures in an image and it is given by

$$I \bullet S = (I \oplus S) \ominus S \quad (5.5)$$

As closing only eliminate image details smaller than the structuring element used. The structuring element is selected such that it covers all possible vascular structures, at the same time preserving the edge of optic disc. In most of the retinal images blood vessels are assumed to be not wider than 15 pixels. Hence, symmetrical disc shaped structuring element of size 15x15 is employed for morphological operation. Figure 5.6 illustrates the gray scale morphology closing result on typical gray level retinal image. Due to dilation operation the small interfering blood vessels are removed. This results in slight blurring of the input image. Next, erosion is done to restore the boundaries to their former position.

5.1.2.2 Boundary Detection Using Geometric Active Contour Model (ACM)

In geometric deformation model the curves are evolved implicitly using geometric computations. The evolving curve is represented as level set function in the image domain . Image segmentation is performed by starting with initial curve and evolving its shape by minimizing energy function represented by level set function. The curve evolution has to stop at the image boundaries where the energy is minimum. Here, a contour is represented by zero level set function and the energy function that is to be iteratively minimized to find the object boundary is given as follows.

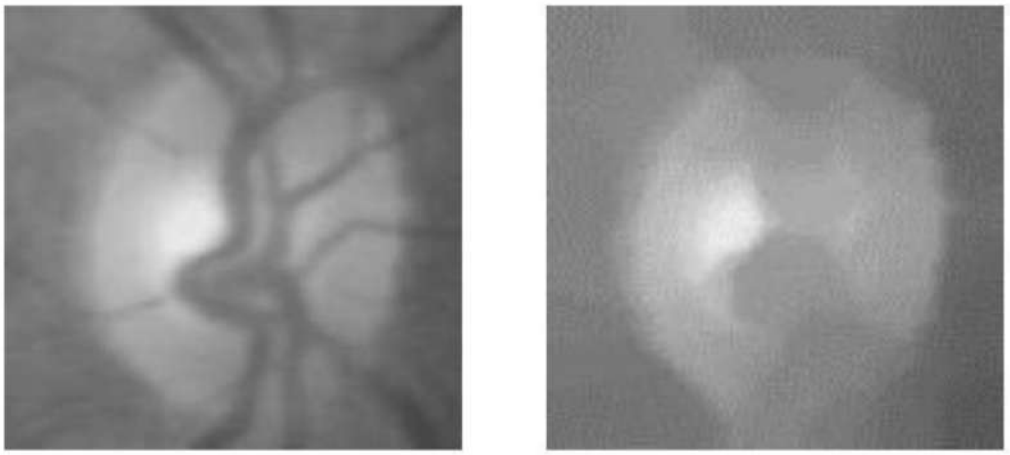

(a) (b)

FIGURE 5.6: Elimination of interfering blood vessels; (a) Optic disc region fragmented by vessels; (b) Morphological closed optic disc region.

$$F_{\emptyset,r_1,r_2} = E_{\emptyset,r1,r_2} + \ell P(\emptyset) + vL(\emptyset) \qquad (5.6)$$

$$P(\emptyset) = \int_{\Omega} \frac{1}{2}(|\nabla\emptyset(x)| - 1)^2 dx \qquad (5.7)$$

$L(\emptyset)$ is the length of zero level curve of $\emptyset$ used to regularize the contour. It is given by

$$L(\emptyset) = \int_{\Omega} \delta(\emptyset(x))|\nabla\emptyset| dx \qquad (5.8)$$

Where $E\emptyset r1, r2$ is the external energy functions ,$\emptyset$ is the zero level set representing contours C in the image domain, $r1$ and $r2$ are two values that fit the image intensities inside and outside the contour respectively. p^Q Is the distance regularizing term used to penalize the deviation of level set $\emptyset$ from a signed distance function it is given by

$ And are positive constants, is the smoothing function called Dirac function. The energy functional (5.6) is to be minimized to find the optic disc boundary. The gradient descent method proposed by Li et al., 2007 is used to minimize the energy function and it is given as follows:

Where 1 and 2 are positive constants, is the Gaussian kernel with localization property with as scaling parameter. And are two values that fit the image intensities inside and

$$\frac{\partial \emptyset}{\partial t} = -\delta(\emptyset)(\alpha_1 e_1 - \alpha_2 e_2) + v\delta(\emptyset)\mathrm{div}\left(\frac{\nabla \emptyset}{|\nabla \emptyset|}\right) + \ell\left(\nabla^2 \emptyset - \mathrm{div}\left(\frac{\nabla \emptyset}{|\nabla \emptyset|}\right)\right) \quad (5.9)$$

The functions e_1 and e_2 are calculated as follows

$$e_1(x) = \int_\Omega k_\sigma(y-x)|I(x) - r_1(y)|^2 dy \quad (5.10)$$

$$e_2(x) = \int_\Omega k_\sigma(y-x)|I(x) - r_2(y)|^2 dy \quad (5.11)$$

outside the contour. The first term equation 5.7 is called data fitting term responsible for driving the active contour toward object boundary. Second term is called length term and it has smoothing effect on contour. Third term is the level set regularization term that controls the speed of contour. Large value of can be used if intensity inhomogeneity is not severe. But it increases the computation time with less iteration required for convergence of active contour to boundary. Increasing the value of v introduces emergence of new contours at boundaries of unwanted structures. Therefore, values of $1, 2, ,$ and O are selected after proper experimentation for the smooth convergence of the active contour to the desired disc boundary.

Once the vascular structures are removed based on the gray scale morphological closing operation, the boundary detection operation is carried out. To fit active contour onto the optic disc the initial contour must be near to the desired boundary otherwise it can converge to the unwanted regions. In order to automatically position an initial contour, the approximate center of optic disc obtained in the localization method is used. A set of points whose distance from the center of optic disc is 50 pixels more than its disc radius are selected. The contour drawn using these points becomes the starting point of the curve. Number of iterations required to detect the boundary of optic disc varies from image to image. In some images only hundred iterations are enough and in some more than hundred iterations are needed. Figure 5.7 shows the convergence of active contour for two different images.

Thus obtained contour specifying the boundary of optic disc is further processed by

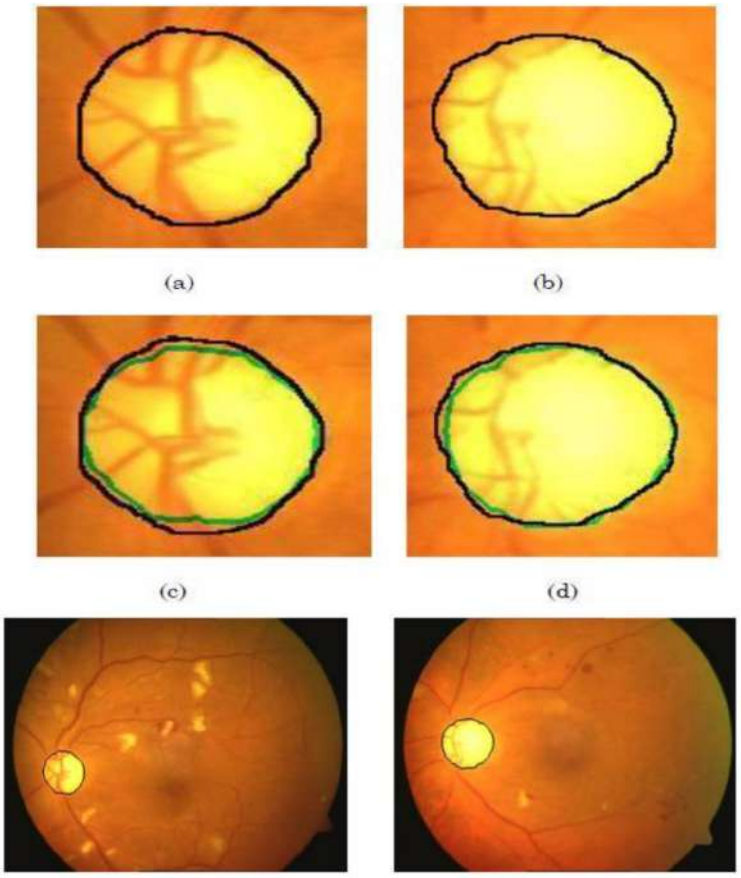

FIGURE 5.7: Geometric active contour based optic disc boundary segmentation; (a) Hand labeled disc boundary of first image; (b) Hand labeled disc boundary of second image; (c)–(d) Automatically detected boundaries (green colour) overlapped on corresponding hand labeled images; (e) Segmented optic disc boundary with 85% sensitivity; (f) Segmented optic disc boundary with 90.78% sensitivity.

dilating it with a small structuring element to avoid discontinuities in the contour. The boundary thus detected is compared with the manually marked optic disc boundary by an expert and results are quantified. Figure 5.8 shows the hand labeled optic disc boundary by an expert and automatically detected optic disc boundary overlapped on the ground truth image in different colour.

5.2 Detection of Macula

The macula is a depression in the center of macular region and appears as a darker area in a colour retinal image. It is located temporal to the optic disc and has no blood vessels present in its center. The fovea central is lies at the center of the macula that is utilized in activities that require discerning sharp details such as reading. Abnormalities

such as exudates present in this region indicate a potential sight threatening condition called maculopathy. The patient may not be aware of the presence of the abnormalities if they are small, but, if left untreated, it results in severe loss of vision. Therefore, it becomes important to detect and mark the macular region in a retinal image for automated detection of abnormalities and their severity level.

In a retinal image, the contrast of macula is often quite low and sometimes it may be obscured by presence of exudates or hemorrhages in its region. As a consequence a search to obtain a global correlation often fails. Therefore, the macula is localized based on its distance and position with respect to the optic disc as it remains relatively constant. The process of detecting the approximate center and diameter of the optic disc has been explained in the earlier sections. Once the optic disc is detected, the macula is localized by finding the darkest region within the specified area in the image. Figure 5.9 illustrates the process of finding the macula in retinal image as follows.

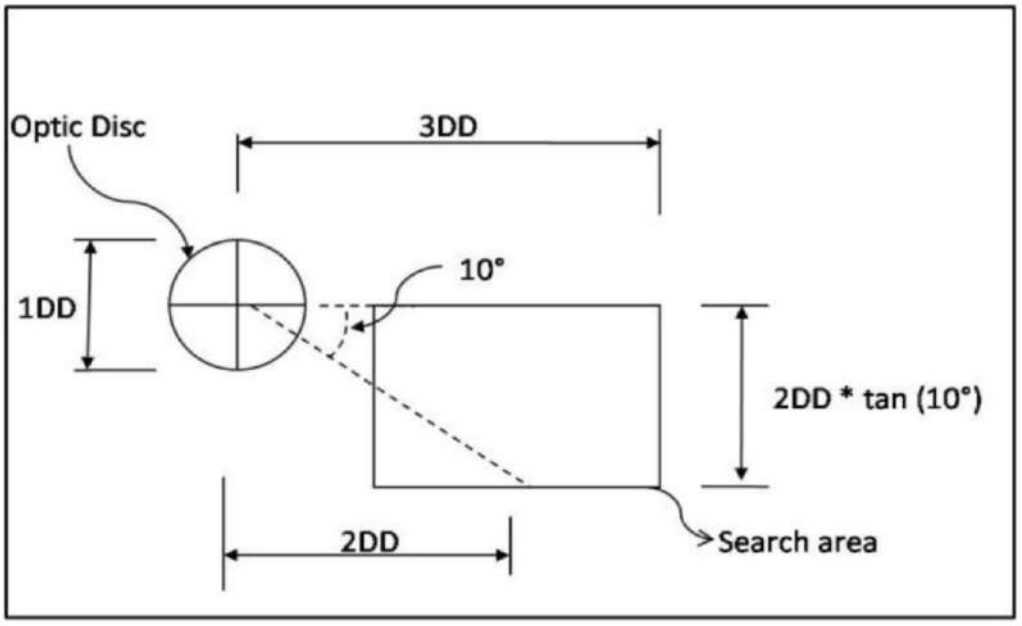

FIGURE 5.8: Illustration of finding a search area to localize macula

Since the location of macula varies from individual to individual, a rectangular search area has to be defined. In a standard retinal image the macula is situated about 2 disc diameter (DD) temporal to the optic disc. Mean angle between the center macula and the center of optic disc against the horizon is found to be about - 5.6 3.3 degrees. Based on this prior knowledge a rectangular search area is formed as shown in Figure 5.9. The width of the search area is taken equal to 2DD as the mean angle between the macula

and the center of the optic disc to the horizontal, as mentioned, varies between -2.3 to -8.9 degrees. A small pixel window of size 4040 is formed to scan the entire area and the average intensity at each pixel location is calculated. The center of the window having the lowest average intensity is taken as the center of the macula. Figure 5.10 shows the result of automatic macula detection method. Once the macula is localized, entire macular region can be determined for detecting the presence or absence of maculopathy.

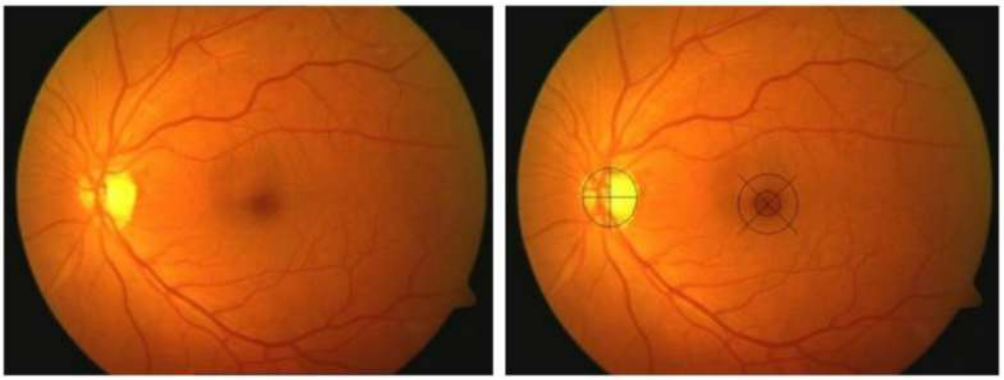

FIGURE 5.9: Automatic localization of macula; (a) Input retinal image; (b) Marked location of macula and optic disc

5.3 Results and Discussion

For the evaluation of automatic localization of optic disc, segmentation of disc boundary and localization of macula a total of 130 digital colour retinal images from DIARETDB0 database are used. Out of these 74 images the optic disc boundary are manually drawn by an expert ophthalmologist as ground truth for disc boundary segmentation method. In optic disc localization, the number of iterations required to calculate the optimal threshold was not more than three for most of the images. The optic disc is located correctly in 125 images out of 130 even in the presence of lesions in the images. For the detection of optic disc boundary initial contour was taken as circle with optic disc center obtained in localization method. All the 74 images were preprocessed with gray morphological closing to eliminate interfering blood vessels. Initial set of points that define contour are automatically selected in the region containing optic disc. As mentioned the size of optic disc diameter in a retina varies from 1.8-2mm (approximately 100 pixels in a standard image). Therefore, a window bigger than this i.e., 150150 pixels is used to

TABLE 5.1: Performance of optic disc localization, macula localization and optic disc boundary detection methods

No. of images	Method	Sensitivity (%)
89	Optic disc localization	99.32
89	Macula localization	96.6
130	Optic disc boundary detection	90.675.05

define a region containing optic disc. Several different values weretested for the parameters of the gradient descent flow equation and it was found the weights $1 = 0.5, 2 = 0.5$ that are integrals over the region outside and inside contour as the best for the retinal images. If 1¿2then it resulted in contour being pulled outwards and if reversed then the contour would converge to regions within optic disc. Value for the length shortening term v was chosen empirically as 66.

Increasing the v resulted in smooth convergence of contour towards disc boundary, but, at the cost of increase in the number of iterations. Scaling parameter was was set to 2.0 as in some images the optic disc region had intensity inhomogeneity. And the regularization value l was set to 1. The number of iterations for convergence of active contour varied from 120 to 200 for different images. Therefore the iteration was set to 200. With these parameter settings the geometric active contour algorithm was applied to 74 images in the dataset. The results were quantified by comparing the segmented disc boundary against the hand labeled ground truth images. Sensitivity is used as the measure to match between two regions in the images. The number of true negatives, that is, the number of pixels not classified as optic disc region pixels, either by human expert or by algorithm is very high. This results in specificity always closer to 100%, that is not meaningful and hence, it is not considered for evaluating the methods. Identification results are summarized in Table 5.1. All the algorithms were realized using Matlab9 and Matlab12 running on 1.66GHz Intel PC with 2GB RAM. And the time taken to detect the optic disc boundary and macula was less than 30 seconds with average sensitivity of 90.675.05 for optic disc boundary detection and sensitivity of 96.6% for macula localization.

5.4 Summary

In this Chapter, efficient methods for the automatic segmentation of optic disc localization, boundary detection and macula localization in colour retinal images are described. Retinal images of patients at different stages of retinopathy were considered to test the robustness of the optimal iterative threshold method followed by connected component analysis in disc localization. In all the images except one the optic disc was located correctly. Localization of disc is important as it has to be masked during the exudates detection and its position is used in the location of macula. Based on the result obtained in optic disc boundary detection, it can be stated that geometric based implicit active contour models provide a better segmentation for images with weak boundaries when compared to parametric models. Shape and size changes in optic disc boundaries can be further studied for the detection of glaucoma. The detection of macula and its region plays an important role in the severity level classification of diabetic maculopathy. Detection of all these features leads towards the development of a fully automated retinal image analysis system to aid clinicians in detecting and diagnosing retinal diseases

Chapter 6

Detection and Grading of Exudative Maculopathy

Diabetic maculopathy is one of the complications of diabetes mellitus that is considered as the major cause of vision loss among people around the world. It results from the leakage of fluid rich in fat and cholesterol from damaged retinal vasculature. Accumulation of these fluids called exudates near the center of the retina, i.e., macula as indicated in the Figure 6.1 leads to distortion of the central vision.

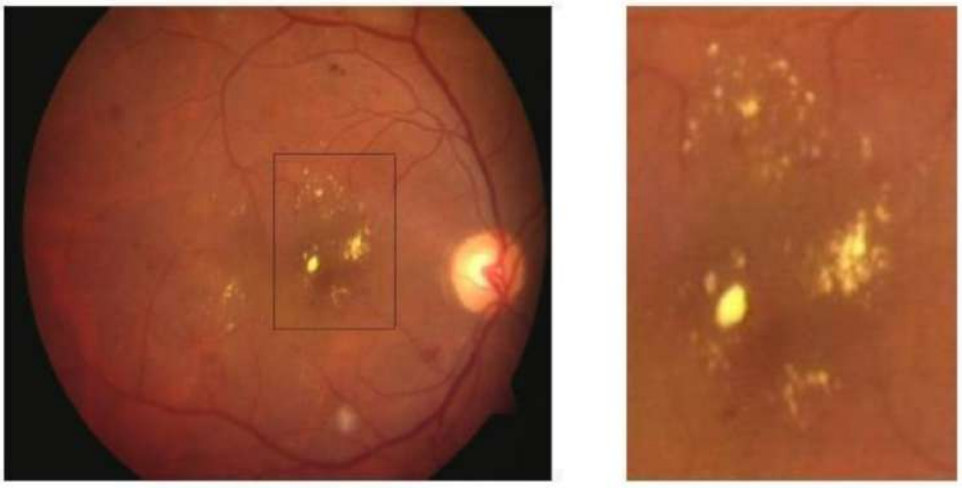

FIGURE 6.1: Diabetic maculopathy condition in color retinal image; (a) Hard exudates in the macular region; (b) Enlarged exudates

Progression of diabetic maculopathy is slow and silent, very often without any symptoms in the early stages. If maculopathy is not detected in the early stage then the damage of the macula or visual field is irreversible and can lead to blindness. Therefore, compulsory regular screening of diabetic eye will help to identify the maculopathy at initial stage and reduce the risk of severe vision loss. Digital screening of maculopathy results in generation of large number of retinal images to be manually analyzed by an expert. This often leads to observer fatigue and increase in the time taken for diagnosis. In this chapter a computer based system for automatic detection and grading of diabetic maculopathy severity level without manual intervention is presented as shown in Figure 6.2. The automatic detection of optic disc and macula are described in the Chapter 5. Optic disc is masked during the detection of exudates. Diameter of the disc and position of macula are used to mark the macular region. Hard exudates are detected using clustering and mathematical morphological techniques. Based on the location of hard exudates in marked macular region the severity level of maculopathy is classified into mild, moderate and severe. Following sections of the Chapter describes these methods in detail. Also, a graphical user interface has been developed for the use of clinicians during the mass screening is explained.

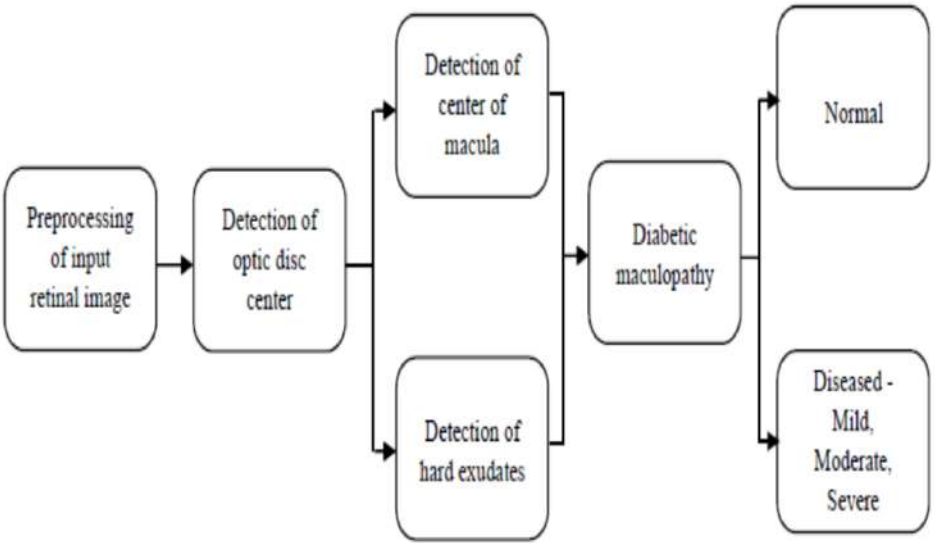

FIGURE 6.2: Automatic diabetic maculopathy severity grading system

6.1 Detection of Hard Exudates

Hard exudates are abnormal lesions caused by diabetic retinopathy in a diabetic's eye. They are associated with patches of retinal vascular damage with leakage. They are considered to be one of the bright intensity regions in the retinal images and appear as random yellowish patches. The size and distribution of exudates may vary during the progress of the disease. The segmentation of hard exudates is achieved in two steps. First, candidate exudate regions are detected using a K- Means clustering method. Afterthis, morphological reconstruction method is applied to find the exact exudate regions. The optic disc which has almost the same intensity as exudates is masked during the exudate detection process to avoid false positives.

6.1.1 Coarse Segmentation of Hard Exudates

Even though hard exudates are considered as bright regions in a retinal image, there are various factors that affect the segmentation of exudates using a single global threshold. For instance, the contrast enhancement algorithm not only enhances the brightness of lesions but also increases the brightness of some pixels. These pixels will be wrongly recognized as lesion pixels. There is also a possibility that segmented image may contain lesions like cotton wools, drusen and pixels surrounding the optic disc. Therefore to classify the segmented region into exudates or non-exudates, K-Means clustering method is employed. In a color retinal image, bright structures like exudates and optic disc appear more contrasted in green channel image as described in Chapter 5. Therefore, only green channel of the original RGB image is used for exudate detection. Initially, a median filter of size 1515 is applied to reduce the uneven illumination in the green channel image. Then, intensity difference image required for the clustering operation is obtained by subtracting the median filtered image from the green channel image as shown in Figure 6.3. This isolates the bright lesions and optic disc regions from the dark background.

The clustering method separates a set of data points into clusters according to the attributes of data. The important measurement of similarity for data is distance between cluster centers and between points inside one cluster. In intensity difference retinal image, the distance measure is the difference in the intensity values between two pixels.

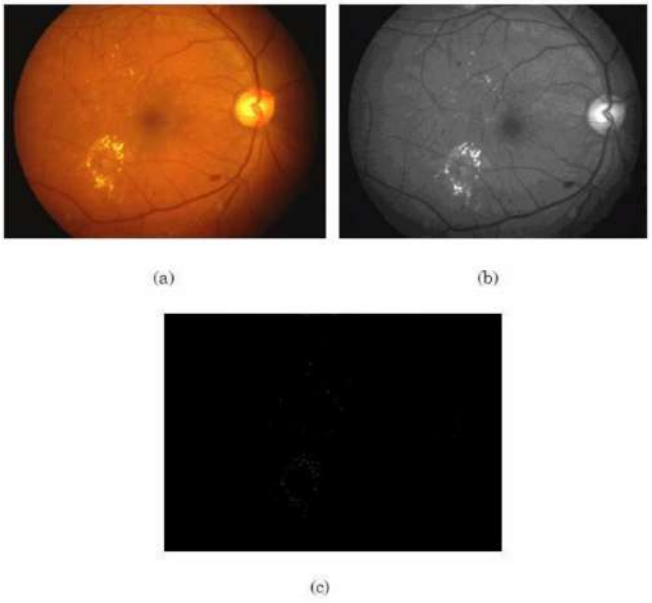

FIGURE 6.3: Creation of intensity difference image for clustering in image space; (a) Colour retinal image; (b) Green channel image; (c) Intensity difference image.

Here, the number of cluster required will be two, i.e., dark background cluster and bright lesion cluster. Exudates cluster will be located in the higher intensity range along with optic disc and other bright lesions and background cluster in the lower intensity range. Initial cluster centroid of exudate cluster CE is set to max, the maximum intensity level in the intensity difference image. And initial cluster centroid of background cluster CB is set to min, the minimum intensity level in the intensity difference image. The clustering performed in the image space is as follows:

- At step k = 1, CE (k) = max, CB (k) = min.
- for i = 1,2,..... mn

  Xi is the intensity level of pixel i

  D1 = distance (Xi, CE (k))

  D2 = distance (Xi, CB (k))

  if D1 ¡ D2

  Pixel i belongs to exudates cluster

  else

  Pixel i belongs to background cluster
- Update cluster centers CE (k+1) and CB (k+1)
- k = k+1 , repeat steps 2 to 4 until stopping conditions is met.

The stopping condition can be that the distance between the two successive cluster centers is not more than user specified value. In this case it was found that maximum of three iterations are enough to separate the candidate lesion regions from the background. Therefore number of iterations was limited not more than three. Figure 6.4 shows the result of clustering in the image space. The optic disc that is part of bright regions is removed from further processing as it may result in false positive. Chapter 5 describes the detection of optic disc region.

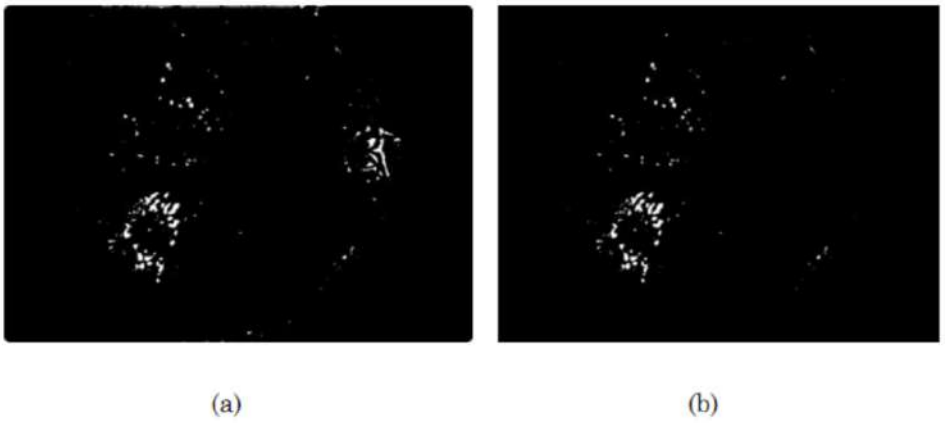

FIGURE 6.4: Coarse segmentation of candidate exudate regions; (a) Cluster of bright pixels separated from background; (b) After removing the optic disc.

6.1.2 Fine Segmentation of Exudates

The segmentation of image by clustering results in number of candidate exudate regions. In order to correctly classify the exudate pixels from the non-exudate pixels, morphological image reconstruction is used. This is an iterative method that extracts regions of interest from an image by repeated dilation on two images, a marker and a mask. Let If be the marker image and Iv be the mask image such that If Iv. Then the conditional dilation operation Ri (If , Iv) is given as follows:

The marker If is allowed to grow in the region by a structuring element B that is restricted by mask Iv. The rough exudate regions obtained from the coarse segmentation are overlaid on the green channel image to get marker image and the original green channel image is used as a mask. The morphological reconstruction by dilation is then applied on the overlaid image. The dilations of marker image under mask image are repeated until the contour of marker image fits under the mask image to get reconstructed

$$R_i(I_f, I_v) = \left(I_f \oplus B\right)\hat{} I_v \qquad (6.1)$$

image. Figure 6.5 shows the difference image obtained by subtracting the morphological reconstructed image from the original image.

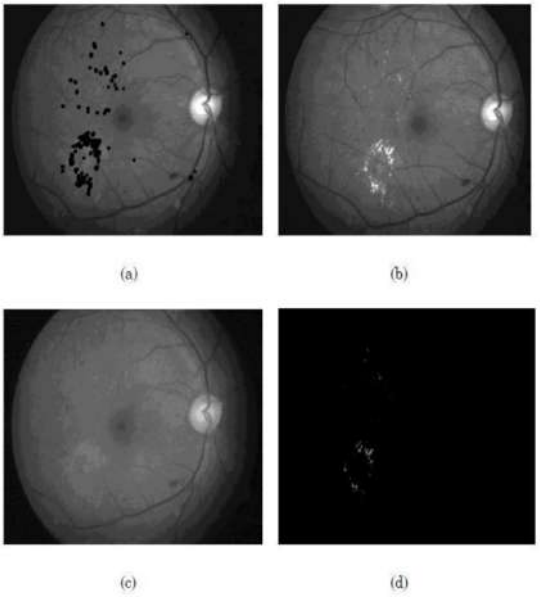

FIGURE 6.5: Morphological reconstruction operation for the segmentation of exudates; (a) Marker image; (b) Mask image; (c) Morphological reconstructed image; (d) Difference image.

A fundus boundary mask is generated for each image as described in the chapter 3. Only those pixels that are inside the fundus mask are considered as exudate pixels. Finally exudate pixels in an image are obtained by thresholding the difference image. The threshold value varies from one retinal image to another. Therefore, a local entropic threshold for each image is calculated as described in the chapter 4. Figure 6.6 shows the final thresholded image and overlapping of detected exudate pixels on the colour retinal image. In the Figure 6.6(d) it can be seen that the cotton wool spot is not detected as exudate region. But, the image variance method results in detection of cotton spot as part of exudate region [37].

i.e (a) Thresholded exudate pixels; (b) Exudates overlaid on original image; (c) Another example of color retinal image; (d) Segmented exudates; (e) Enlarged view of detected exudates

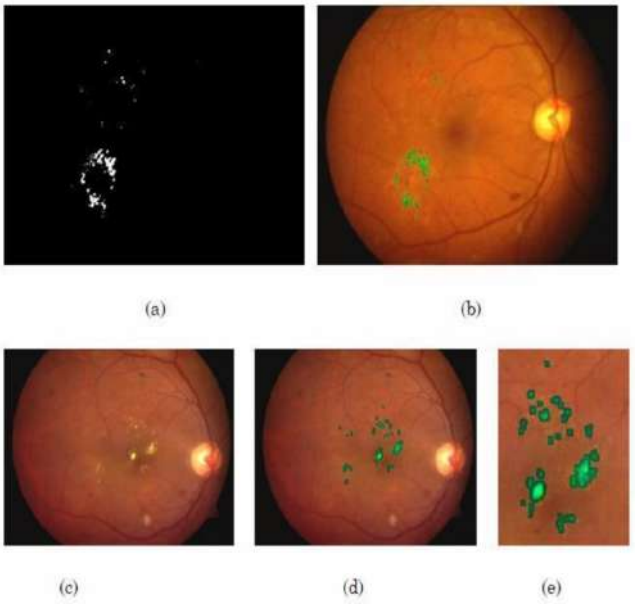

FIGURE 6.6: Fine segmentation of hard exudates

6.2 Automatic Severity Level Grading of Diabetic Maculopathy

Diabetic maculopathy is the condition of retinopathy where exudates are present within the macular region. Severity of the maculopathy depends on how close exudates are to the center of macula. In the CSME stage, most of the retinal blood vessels are damaged and the leakage area becomes bigger. The exudates leak out and this liquid concentrates very close to the fovea. The visibility is greatly affected as the image cannot be focused on the macula properly. The condition where the locations of exudates are far away from the center and outside the macular region is sometimes called clinically non-significant macular edema. Here the patient will not realize that he is affected as there are no visible symptoms. The severity level in CSME is classified as mild, moderate and severe based on the international grading standard. In an attempt to improve the communication worldwide between ophthalmologists and primary care physicians caring for patients with diabetes, an international clinical disease severity scale was recently developed as shown in Table 6.1. In this work, automatic grading of diabetic maculopathy is done according to this standard diabetic macular edema disease severity scale. This scale is based on the Early Treatment of Diabetic Retinopathy Study (ETDRS) classification of diabetic retinopathy. ETDRS has been set to assign a severity level based on evaluation

TABLE 6.1: International clinical diabetic macular edema severity scale

Proposed Disease Severity Level	Findings Observable upon Dilated Ophthalmoscope
Diabetic macular edema apparently absent. Diabetic macular edema apparently present.	No hard exudates in posterior pole Some exudates in posterior pole
If diabetic macular edema is present, it can be categorized as follows:	
Proposed disease severity level	Findings observable upon dilate ophthalmoscopy
Diabetic macular edema present	Mild diabetic macular edema: some hard exudates in posterior pole but distant from the center of the macula (>1DD and <2DD)
	Moderate diabetic macular edema: Hard exudates approaching the center of the macula but not involving the center (>1DD and >1/3 DD)

of stereo retinal images of people suffering from diabetic retinopathy, and is described as the gold standard for early detection and treatment.

After the detection of hard exudates, the macula is located based on its relative position from the optic disc as described in the chapter 5. The macular region is then divided into three marker regions using three circles with radii 1/3 of optic Disc Diameter (DD), 1 DD and 2 DD centered at macula. In any given image if the exudates are absent, then it is classified as normal without any maculopathy (Figure 6.7(a)). If exudates are present and are outside the 2DD region then it is classified as clinically non-significant macular edema. Presence of exudates within the 2DD is classified as clinically significant macular edema and it has to be treated by laser. In case of CSME, the presence of exudates outside the 1DD region is termed as mild (Figure 6.7(b)). The moderate case is one with presence of exudates within the 1DD region not involving the center of the macula called foveola, i.e., outside the circle of 1/3 DD (Figure 6.7(c)). In severe case, the exudates are present inside the 1/3 DD region obscuring the center of macula (Figure 6.7(d)). This is the most sight threatening stage of maculopathy where vision is significantly reduced. Figure 6.7 shows the results of the automatic maculopathy detection and grading system without any manual intervention. It can be seen that the results provide a valuable aid for the clinician in identifying severity level of the disease.

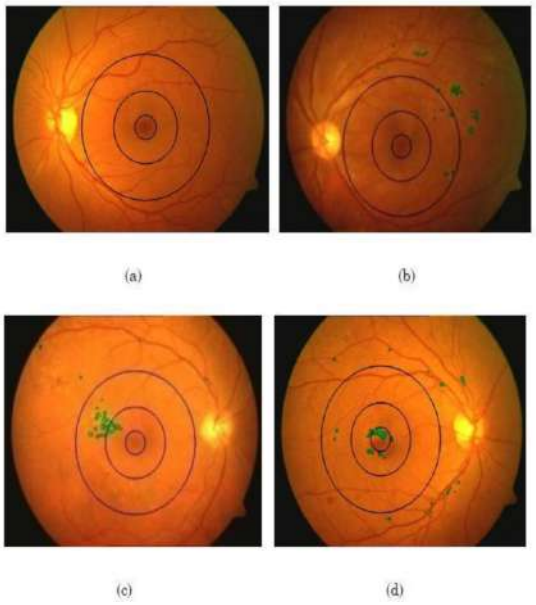

FIGURE 6.7: Exudative maculopathy severity grading; (a) Normal; (b) Mild stage; (c) Moderate stage; (d) Severe stage of maculopathy.

6.3 Graphical User Interface for Automatic Detection of Retinal Features

A graphical user interface has been implemented in Matlab9 and Matlab12 using Graphical User Interface Development Environment (GUIDE). It can be initialized through its main window (Figure 6.7). The interface currently comprehends:

- Selecting and opening the retinal images from three different databases. DRIVE and STARE retinal databases. The DRIVE and STARE databases are mainly used for the detection and evaluation of retinal vessel extraction method.
- Option to find the location and diameter of optic disc. Also its exact boundary can be detected.
- Option to find the macula and to automatically draw macular region is provided. v Retinal blood vessels can be segmented using the Gabor filter based method as described in the Chapter 4. The performance of vessel extraction method can be observed using sensitivity and specificity as evaluation parameters.
- Hard exudates detection method is provided.

- Option for automatic detection and severity level grading of diabetic maculopathy is provided.
- Option to save the result images for further analysis is provided.

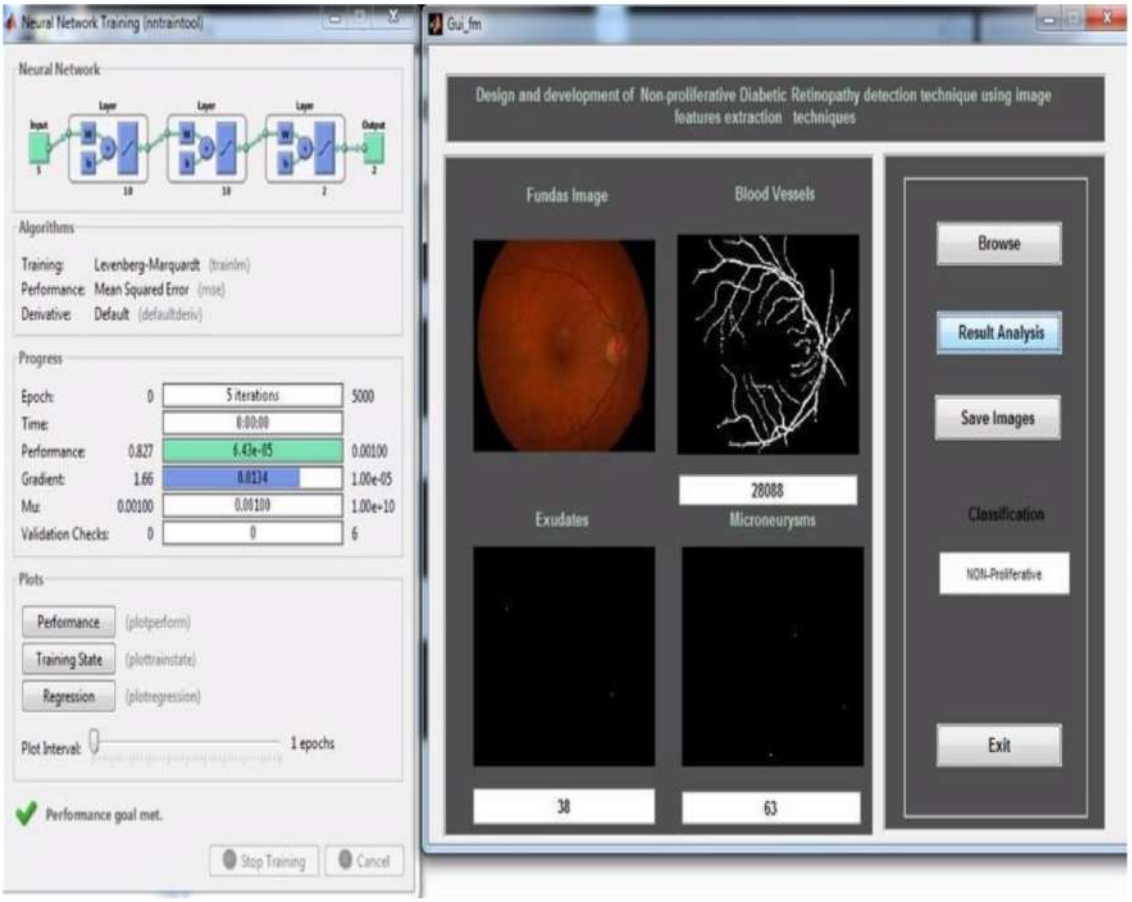

FIGURE 6.8: GUI for the automatic identification of features in colour retinal images.

6.4 Results and Discussion

For the evaluation of automatic grading of diabetic maculopathy, 130 digital color retinal images were used from DIARETDB0 dataset. Among these, 52 are normal retinal images without any signs of maculopathy and 96 images are identified as clinically significant macular edema images by an ophthalmologist. Another dataset called Diaretdb1 was used for evaluating the hard exudate detection method. This dataset provided 88 color retinal image along with information of presence or absence of exudates in image. Image based sensitivity and specificity is used to evaluate the performance of the exudate detection method and it is summarized as shown in Table 6.2. In DIARETDB0 database,

Table 6.2: Performance of hard exudates detection method

Database	No. of images	No. of normal images	No. of images with exudates	Sensitivity (%)	Sensitivity (%)
Database	130	62	96	97.9	96.1
Diaretdb1	80	45	43	93	97-7

Table 6.3: Performance the maculopathy severity grading

No. of images	True positive	True negative	False positive	False negative	Sensitivity (%)	Sensitivity (%)
130	87	50	2	4	95.6	96.15

the hard exudates were detected correctly in 94 images with sensitivity of 97.9%. Out of 52 normal images two were classified as diseased with the specificity of 96.1%. The wrong classification was a result of high brightness in an image due to over exposure of the retina during the imaging.

Center of macular region was not detected properly in five images due to the poor contrast in the image and these were not considered to evaluate the automatic grading of maculopathy. The exudates detection method was tested on Pentium PC with 1.66 GHz and 2GB memory using Matlab9 and Matlab12. Each image took less than a minute to find the exudate regions. The result of the exudates detection was superimposed on the original image and it was found that the previously unclear exudate regions were visibly highlighted and aided clinicians to identify pathology in less time. The overall performance of the system to automatically detect the maculopathy stages is given in the Table 6.3. Total of 130 images were considered from the database. Five images were not considered as the macula center was not detected properly due to the poor image quality. 91 images with different level of Exudative maculopathy and 52 normal images were considered for the evaluation. The overall sensitivity of 95.6% and specificity of 96.15% was achieved.

For the statistical significance analysis of maculopathy severity level detection method, the area covered by the exudates in three circular regions R1, R2 and R3 centered at macula as in Figure 6.9 is considered.

Based on the presence of hard exudates in the marked macular regions, Table 6.4 gives the distribution of exudates in the macular regions for the classification of maculopathy severity level.

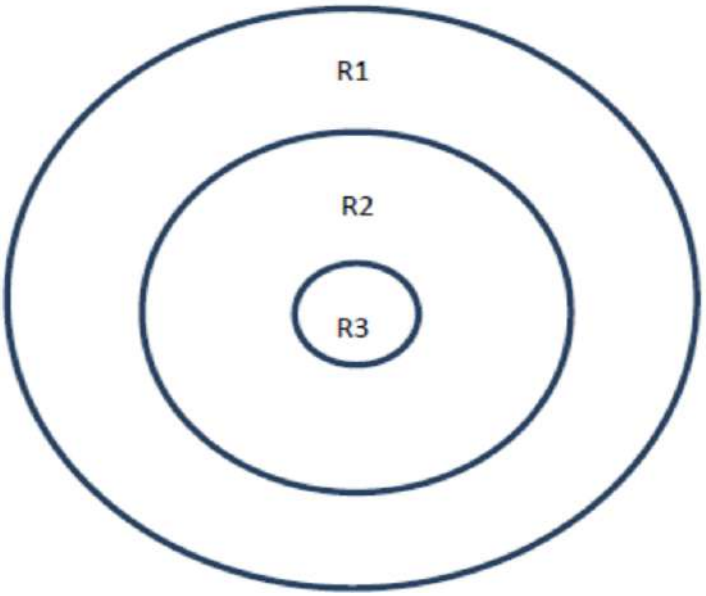

FIGURE 6.9: Illustration of macular regions

TABLE 6.4: Classification of maculopathy severity level

Severity level	Hard exudates		
	R1	R2	R3
Mild	Present	Absent	Absent
Moderate	Present/Absent	Present	Absent
Severe	Present/Absent	Present/Absent	Present

Total area of the hard exudates in region R1, R2 and R3 are found for different severity levels. This data is subjected to ANOVA (Analysis of Variance between the three groups) to test the statistical significance. But for the data presented for the test in this case, the normality assumption is violated. That is, data is not normally distributed; this is due to large variations in the pixel values within the groups. Therefore, Kruskal-Wallis rank test, a non-parametric procedure has been used for testing clinical significance as follows. Kruskal-Wallis test is an alternative to the one-way ANOVA F test. Instead of comparing each of the group means against grand mean, the Kruskal-Wallis test compares the mean rank in each of the groups against the overall mean rank. If there is a significant difference among the different groups, the mean rank differs considerably from group to group. In process of squaring these differences, the test statistic H becomes large. If there are no differences present, the test statistic H is small because the mean of the ranks assigned in each group should be very similar from group to group. The equation 1, defines the Kruskal-Wallis test statistic, H.

To illustrate the Kruskal-Wallis test for differences among 3 medians, we consider the

$$H = \left[\frac{12}{n(n+1)}\sum_{j=1}^{c}\frac{T_j^2}{n_j}\right] - 3(n+1) \qquad (6.2)$$

TABLE 6.5: Exudates area in three regions of severe maculopathy

R1	R2	R3
160	759	816
153	552	723
3324	546	212
1467	827	711
856	1927	394
0	151	276

following data for severe maculopathy as in Table 6.5. Similarly data for mild and moderate maculopathy are also prepared.

Define Null hypo Dissertation H0 and Alternate hypo Dissertation H1 to start the test.

- H0: There is no difference between the regions
- H1: There is a difference between the regions (at least one of the region differs from others)

The Alpha value at start is considered to be = 0.05, and the degrees of freedom is 2. The test statistic, H, is approximated by chi-square distribution. It is found that for a given alpha value 0.05 and degrees of freedom 2, the critical value 2 is 5.99147. Therefore, the decision rule is

- Reject H0 if H ¿ 2
- Otherwise do not reject H0

The statistic H approximately follows a chi-square distribution with C-1 degrees of freedom. Using a 0.05 level of significance, 2, the critical value of the chi-square distribution with C-1 = 2 degrees of freedom is 5.99147.

Because the computed value of the test statistic H = 7.162 is greater than the critical value, the null hypo Dissertation is rejected and conclude that there is a difference between the regions with respect to number of exudate pixels. The same conclusion is reached by using the p-value approach. Here, the p-value = 0.0278 ¡ 0.05, indicating

TABLE 6.6: Kruskal-Wallis Rank test for statistical significance of maculopathy severity levels

Severity level	Average Rank			Test Statistic	p-value
	R1	R2	R3		
Mild	38	15.5	15.5	29.34	$p<0.05$
Moderate	71	50	15.5	69.03	$p<0.05$
Severe	36	33	22	7.162	$p<0.05$

that it is clinically significant. The Table 6.6 shows the Kruskal- Wallis test performed on the mild, moderate and severe level of exudative maculopathy. Based on the result it is seen that there is significance difference between at least two regions. The results obtained from the methods are also in accordance with the standard. It states that a minimum standard of 80% sensitivity and 95% specificity is to be achieved by any automatic method for the detection of diabetic related eye disease. The result obtained from the work has met the requirement. The graphical user interface developed can be used by clinicians during the mass screening of diabetic retinopathy.

6.5 Summary

In this Chapter, the development of automatic retinal image processing system for detection and grading of maculopathy has been described. For the automatic detection of maculopathy two features in retinal image are needed. One is the macula, based on its position and optic disc diameter, macular region has been drawn. Another feature is hard exudates. The coarse segmentation of exudates, which was achieved using K-Means clustering provided a better initial coarse segmentation when compared with the variance based method proposed in the literature. In variance based segmentation cotton wools were considered as part of exudates. This resulted in classifying cotton wool spots as exudates in the end result. Also automatic threshold calculation after morphological reconstruction was important, and it was achieved with entropic thresholding. The existing models of retinal screening are expensive, time consuming and require trained ophthalmologists. The developed automatic system was able to detect diabetic maculopathy and its severity level in less time. The sample image data used to validate this software was comparable across manual graders with regard to the distribution of severity of the disease. It also provides a user interface for speedy analysis of large

number of retinal images during the mass screening of diabetic related eye diseases. It is hoped that this system can assist the ophthalmologists to detect the signs of diabetic retinopathy in the early stage, in disease monitoring and for a better treatment plan.

Chapter 7

Conclusion

This Dissertation has considered the new methods for the automatic identification of anatomical features like optic disc, blood vessels, macula and pathological feature like hard exudates in digital colour retinal images. This has led to the development of computer based system for detection and severity level grading of diabetic maculopathy. The system finds its direct application during the screening of eye diseases for ever increasing diabetic population.

A general introduction of the potential and challenges of retinal image analysis was first presented in Chapter 1. With digital retinal imaging playing an increasingly prominent role in the diagnosis and treatment of eye diseases, the problem of extracting clinically useful information has become important. For example, retinal vasculature, optic disc boundary, macula and location of exudates help to define the character and extent of diseases like diabetic retinopathy and glaucoma, aiding diagnosis and treatment. Therefore, segmentation of these features becomes a key challenge for proper analysis, visualization and quantitative comparison. This has been the main focus of this dissertation, i.e., segmentation of normal and abnormal features in colour retinal images. The Chapter 2 provided a review of common segmentation algorithms for retinal image features. From both number and diversity of algorithms used for retinopathy detection it was clear that there is no gold standard which solves entire problem.

Chapter 3 has been devoted to the preprocessing and description of retinal image databases used to evaluate the methods. The database obtained from DIARETDB0 HAS a very large variability in terms of disease and image quality. Some of the images

were discarded by ophthalmologists prior to the diagnosis. But such images were included in the database to check the robustness of the developed system. Images that suffered from non-uniform illumination and poor contrast were subjected to preprocessing, before subjected to segmentation. Colour normalization was performed to attenuate colour variations in the image by normalizing the colour of the original retinal image against a reference image. In order to correct non uniform illumination and to improve contrast of an image, contrast-limited adaptive histogram equalization was used. These preprocessing steps were found to improve the segmentation results of optic disc and exudates. For each image in the database fundus mask was detected, that facilitated the detection of vessels and exudate pixels within the region of interest.

The segmentation of blood vessels in colour retinal images using Gabor filters has been described in Chapter 4. It was found that the appearance of vessels is highly sensitive in the gray scale image containing only the wavelength of green. Therefore, for segmentation of vessels was performed using only green channel of RGB colour image. Gabor filter, whose application can be found in problems such as, strokes in character recognition and detecting roads in satellite image analysis, were explored to detect and enhance vessel features in retinal image. When compared with the matched filter for detecting line like features, Gabor filter provided a better result as it has optimal localization in both the frequency and space domains. The Gabor filter was tuned to a suitable frequency and orientation was able to emphasize vessels along that direction and filtering out background noise and other undesirable structures. Values of all the filter parameter were selected based on the properties of vessels. When filter was aligned along orientation of vessel it produced single peak response along that direction. Bank of 12 Gabor filters oriented along different directions in the range of 0 to 170 degrees were used to enhance the multi-oriented vessels. Increasing the number of filter banks did not result in significant improvement of result but increased the time consuming convolution operation. The resulted enhanced vessels were then subjected to thresholding for vessel pixel classification. Entropic threshold calculation based on gray level co-occurrence matrix as it contained information on the distribution of gray level frequency and edge information have been presented. Two publicly available databases were used to evaluate the performance of the method and also to compare it with the matched filter methods. It was found that for DRIVE database the method provided sensitivity of 86.473.6% and 961.01 specificity. And for the STARE database 85% sensitivity and 96% specificity

were achieved. It was found that the number of miss classified pixels was less compared to matched filter methods using the same database.

Segmentation of optic disc boundary and localization of macula has been discussed in Chapter 5. Detection of these two features of retina was necessary for the proper detection of exudates and also for knowing the severity of the diabetic maculopathy. Based on the fact that optic cup part of the disc being the brightest part in the image, optimal thresholding technique was employed to calculate initial threshold. After experimenting with individual red, green and blue channel of RGB colour image, it was found that gray scale image containing green channel provide better result when subjected to thresholding. The interfering vessels in the optic disc made the process of finding the approximate center of disc complicated. Fragmented optic disc regions had to be merged to get the center of the disc. According to the prior information about the diameter of optic disc in a standard retinal image, connected components and iterative thresholding was used to locate optic disc. The macula was localized based on its distance and position with respect to the optic disc as it remained relatively constant. Even though macula is considered to be one of the darkest regions without vessels in a retinal image, less contrast between the macula and background makes it difficult to locate based on image variance. Therefore, a rectangular region was formed as a search area to locate the macula in an image. Among 130 images considered for evaluating the methods optic disc and macula were localized with sensitivity of 99.32% and 96.6% respectively.

Detection of optic disc boundary becomes important for the diagnosis of glaucoma. Difficulty in finding the optic disc boundary is due to its highly variable appearance in retinal images. Geometric active contour model was explored to segment the optic disc boundary as classical segmentation algorithms failed to provide good result. Image segmentation was performed by starting with initial curve and evolving its shape by minimizing energy function represented by level set function. The iterative curve evolution was stopped at the image boundaries where the energy was minimum. Experiment was performed on both RGB image and gray scale image and found that implicit active contours provided better result with gray scale images. Total of 89 images were used to evaluate the method. Optic disc boundary drawn manually by an expert was used as ground truth. The method was able to achieve average sensitivity of 90.67% with mean of 5.05. Based on the result obtained in optic disc boundary detection, it can be stated

that geometric based implicit active contour models provide a better segmentation for images with weak boundaries when compared to parametric models.

The detection of hard exudates in retinal images and development of automated system for the detection of diabetic maculopathy has been described in Chapter 6. Hard exudates that are responsible for exudative maculopathy was detected using two levels of segmentation for improved accuracy. The coarse segmentation of exudates that was achieved using K-Means clustering provided a better initial coarse segmentation when compared with the variance based method proposed in the literature. Fine segmentation using morphological reconstruction technique classified the correct exudate pixels from the background. Also, automatic threshold calculation after morphological reconstruction is important, and it was achieved with entropic thresholding, thus making the method to work without manual intervention. Total of 130 images from DIARETDB0 database and 89 images from Diaretdb1 database were used to evaluate the method. Average image based sensitivity of 97.9% and specificity of 96.1% was achieved for DIARETDB0 database. And 93% sensitivity and 97.7% specificity was achieved for Diabetdb1 database. Based on the location of exudates in the macular region, the severity levels of diabetic maculopathy were classified into mild, moderate and severe. The existing models of retinal screening are expensive, time consuming and require trained ophthalmologists. The developed automatic system is able to detect diabetic maculopathy and its severity level in less time. The sample image data used to validate this software was comparable across manual graders with regard to the distribution of severity of the disease. An overall sensitivity of 95.6% and specificity of 96.15% was achieved by the system. Graphical user interface was also developed for assisting the clinicians during the screening process. The results proved that it is possible to use the developed algorithms for assisting an ophthalmologist to segment fundus images into normal regions and lesions, and thus support the ophthalmologist in decision making.

7.1 Contributions of the Dissertation

The major contributions of this dissertation can be summarized as:

- The development of new methods for the detection of the following three anatomical structures in retina.

- Automatic localization of optic disc using optimal threshold and connected component analysis. And optic disc boundary detection using geometric based active contour model.
- Automatic localization of macula.
- Automatic segmentation of retinal blood vessels using Gabor filters and entropic thresholding.
  - Automatic detection of hard exudates in retinal image for the detection of diabetic retinopathy.
  - The development of computer based system for automatic detection and severity level classification of diabetic maculopathy. Also development of GUI for assisting ophthalmologists during screening process.
  - As compare to earlier work image based sensitivity of 97.9% and specificity of 96.1% was achieved for DIARETDB0 database. And 93% sensitivity and 97.7% specificity result has been improved was achieved for Diabetdb1 database.

7.2 Future Direction

Although the results presented here have demonstrated the effectiveness of the proposed methods, there is still a lot of scope for improvement in the automatic retinal image analysis system. The segmentation of retinal vessels can further be used for number of purposes. The retinal vascular toruosity is shown to become a predictive factor for cardiovascular diseases and diabetes. The changes in retinal vascular toruosity might be a sign of severity or improvement of the disease. A new technique to analyze and quantify toruosity by considering vessel segment's width has to be found. For the registration of images of patient taken over a time or acquired using different modalities, the retinal vessel branching points can be used as control points that are to be mapped in two images.

As described earlier, the changes in the shape and size of optic disc can be used to detect and diagnose sight threatening disease called glaucoma. The method has to be further

improved to detect optic cup part of the disc, so that changes in the disc to cup ratio can be used as a measure of glaucoma.

Detection and classification of diabetic retinopathy has to be improved by identifying other types of lesions like, hemorrhages, microaneurysms and cotton wool spots. Hard exudate detection has to be improved further by considering other clustering techniques. The system developed so far is capable of detecting maculopathy. It has to be further developed to include detection and severity of retinopathy. Finally, a feature to embed patient diagnosis information within the image will be beneficial.

Chapter 8

Bibliography

1. Kaur, Jaspreet, and H. P. Sinha. "Automated localisation of optic disc and macula from fundus images." International journal of Advanced research in computer science and software engineering 2.4 (2012).

2. Gonzales R. C., and Woods R. E., —Digital image processing, 2nd Edition, Pearson Education, pp. 94-101, 2004.

3. Abramoff D. M., Niemeijer M., Suttorp-Schulten, Viergever A. M., Russell R.S., and Van Ginneken B., —Evaluation of a system for automatic detection of diabetic retinopathy from color fundus photographs in a large population of patients with diabetes, Diabetes Care, vol. 31, no. 2, pp. 193-198, 2008.

4. L. Gagnon*a, M. Lalonde*a, M. Beaulieu*a, M.-C. Boucher**b"Procedure to detect anatomical structures in optical fundus images" a Computer Research Institute of Montreal; bDept. Of Ophthalmology, Maisonneuve-Rosemont Hospital, Proceedings of the Conference Vision Interface 2000, 61-68, 2000.

5. MGoldbaum, Michael, et al. "Automated diagnosis and image understanding with object extraction, object classification, and inferencing in retinal images." Proceedings of 3rd IEEE International Conference on Image Processing. Vol. 3. IEEE, 1996.

6. Mead A., Burnett S., and Davey C., —Diabetic retinal screening in UK, Journal of Royal Society of Medicine, vol. 94, no. 3, pp. 127129, 2001.

7. Khurana A. K., —Comprehensive Ophthalmology, 4th Edition, New Age International Publisher‘s Ltd, India, 2007.

8. Sachin R. K., and L. D. Sota, —Diabetes and eye, Medi-focus, vol. 6, no. 1, pp. 8, 2007.

9. Rakhi D., Lalit D., Rajesh K. J., Catherin A. M., and Gullapalli N., —Awareness of eye diseases in an urban population in southern India, Bulletin of World Health Organization, vol. 79, no. 2, pp. 96-102, 2001.

10. Akita K., and Kuga H., —A computer method of understanding ocular fundus images, Pattern Recognition, vol. 15, no. 6, pp. 431–443, 1982.

11. Al-Rawi M., Qutaishat M., and Arrar M., —An improved matched filter for blood vessel detection of digital retinal images, Computers in Biology Medicine, vol. 37, no. 2, pp. 262-267, 2007.

12. Bone H., Steel C., and Steel D., —Screening for diabetic retinopathy, Optometry, vol. 6, no. 10, pp. 40-43, and 2004.

13. Chang C. I., Du Y., Wang J., Guo S. M., and Thouin P. D., —Survey and comparative analysis of entropy and relative entropy thresholding techniques, IEE Proceedings of Vision, Image and Signal Processing, vol. 153, no. 6, pp. 837-850, 2006.

14. Chanwimaluang T., and Fan G., —An efficient algorithm for extraction of anatomical structures in retinal images, Proceedings of International Conference on Image Processing, vol. 1, pp. 1093-1096, 2003.

15. Chaudhuri S., Chatterjee S., Katz N., Nelson M., and Goldbaum M. —Detection of blood vessels in retinal images using two dimensional matched filters, IEEE transactions on Medical Imaging, vol. 8, no. 3, pp. 263–269. 1989a.

16. Kanski J., Diabetic Retinopathy, Clinical Ophthalmology, Butterworth-Heimann, Oxford Press. 1997.

17. Smith T. S., Szetu J., and Bourne R. R, —The prevalence and severity of diabetic retinopathy, associated risk factors and vision loss in patients registered with type 2 diabetes in Luganville, Vanuatu, British Journal of Ophthalmology, vol. 91, no. 4, pp. 415-419, 2007.

18. McGavin M., —Diabetes and diabetic retina, Community Eye Health Journal, vol. 9, no. 20, pp. 49-50, 1996.

19. Shah P., Jacks A., and Khaw P., —Eye disease in clinical practice: A concise colour atlas, Manticore Books. 2000.

20. Chowdhury T. A., Hopkins D., and Dodson P. M., —The role of serum lipids in exudative diabetic maculopathy: is there a place for lipid lowering therapy, Eye, vol. 16, pp. 689-693, 2002

21. Zander E., Herfurth S., Bohl B., Heinke P., Herrmann U., and Kohnert K., —Maculopathy in patients with diabetes mellitus type 1 and type 2: associations with risk factors, British Journal of Ophthalmology, vol. 84, no. 8, pp. 871–876, 2000.

22. Facey, K., Cummins, E., Macpherson, K., Reay, L., and Slattery, J., —Organisation of Services for Diabetic Retinopathy Screening: Health Technology Assessment Report 1, Health Technology Board for Scotland, pp. 231-273, 2002.

23. Fransen S., Leonard-Martin T., Feuer W., and Lloyd Hildebrand P., —Clinical evaluation of patients with diabetic retinopathy Ophthalmology: accuracy of the Inoveon Diabetic Retinopathy3DT System, Ophthalmology, vol. 109, no. 3,pp. 595–601, 2002

24. Hansen A., Hartvig N., Jensen M., Borch-Johnsen K., Lund Andersen H., and Larsen M., Diabetic retinopathy screening using digital non-mydriatic fundus photography and automated digital analysis, Acta Ophthalmologica Scandinavica, vol. 82, no. 6, pp. 666–672, 2004.

25. Dougherty G., Johson M. J., and Wiers M., —Measurement of retinal vascular tortuosity and its application to retinal pathologies, Journal of Medical Biological Engineering Computing, vol. 48, no. 1, pp. 87-95, 2010.

26. Laliberte F., Gagnon L., and Sheng Y., —Registration and fusion of retinal images: An evaluation study, IEEE Transactions on Medical Imaging, vol. 22, no. 5, pp. 661–673, 2003.

27. Ritter N., Owens R., Cooper J., Eikelboom R. H., and van Saarloos P. P., —Registration of stereo and temporal images of the retina, IEEE Transactions on Medical Imaging, vol. 18, no. 5, pp. 404-418, 1999.

28. Kubeka L., and Jan L., —Registration of biomedical retinal images-improving modifications, Proceedings of IEEE International Conference on Engineering in Medicine and Biology, pp. 1695-1698, 2004.

29. Chaudhuri S., Chatterjee S., Katz N., Nelson M., and Goldbaum M., —Automatic detection of the optic nerve in retinal images, Proceedings of the IEEE International Conference on Image Processing, vol. 1, pp. 1–5. 1989b.

30. Patton N., Tariq M. A., MacGillivrayd T., Dearye I. J., Baljean D., Robert H. E., Kanagasingam Y., and Constable J., —Retinal image analysis: Concepts, applications and potential, Progress in Retinal and Eye Research, vol. 25, no. 1, pp. 99-127, 2005.

31. Teng T., Lefley M., and Claremont D., —Progress towards automated diabetic ocular screening: a review of image analysis and intelligent systems for diabetic retinopathy, Journal of Medical Biological Engineering Computing, vol. 40, no. 1, pp. 2–13. 2002.

32. Heneghan C., Flynn J., O'Keefe M., and Cahill M,— Characterization of changes in blood vessel width and tortuosity in retinopathy of prematurity using image analysis, Medical Image Analysis, vol. 6, no. 4, pp. 407–429, 2002.

33. Hoover A., Kouznetsoza V., and Goldbaum M., —Locating blood vessels in retinal images by piecewise threshold probing of a matched filter response, IEEE Transactions on Medical Imaging, vol. 19, no. 3, pp. 203–210, 2000.

34. Yang C. W., Ma D. J., Chao S. C., Wang C. M., Wen C. H., and Lo S. C., et al. —A computer aided diagnostic detection system of venous beading in retinal images, Optical Engineering, vol. 39, no. 5, pp. 1293–1303, 2000.

35. Pinz A., Bernogger S., Datlinger P., and Kruger A., —Mapping the human retina, IEEE Transactions on Medical imaging, vol. 17, no. 4, pp. 210-215, 1998.

36. Kochner B., Schulmann D., Michaelis M., Mann G., and Englemeier K. H., —Course tracking and contour extraction of retinal vessels from colour fundus photographs: most efficient use of steerable filters for model based image analysis, Proceedings of the SPIE Conference on Medical Imaging, vol. 3338, pp. 755– 761, 1998.

37. Frame A., McCree M., Olson J., McHardy K., Sharp P., and Forrester J.V., —Structural analysis of retinal vessels, Proceedings of the 6th International Conference on Image Processing and its Applications, vol. 2, pp. 824–827, 1996.

38. Fong D., Aiello L., Gardner T., and King G., —Diabetic retinopathy, Diabetes care, vol. 26, no. 1, pp. 99-102, 2003.

39. Sinthanayothin C., Boyce J. F., Cook H. L., and Williamson T. H., —Automated location of the optic disc, fovea, and retinal blood vessels from digital color fundus images, British Journal of Ophthalmology, vol. 83, no. 8, pp. 902–910, 1999.

40. Soares J. V. B., Leandro J. J. G., Cesar R. M, H. F. Jelinek., and Cree M. J., —Retinal vessel segmentation using the 2-D Gabor wavelet and supervised classification, IEEE Transactions on Medical Imaging, vol. 25, no. 9, pp. 1214–1222, 2006

41. Hoover A., Kouznetsoza V., and Goldbaum M., —Locating blood vessels in retinal images by piecewise threshold probing of a matched filter response, IEEE Transactions on Medical Imaging, vol. 19, no. 3, pp. 203–210, 2000.

42. Zana F., and Klein J., —A multimodal registration algorithm of eye fundus images using vessels detection and Hough transform,IEEE Transactions on Medical Imaging, vol. 18, no. 5, pp. 419– 428, 1999

43. Walter T., Klein J. C., Massin P., and Erginay A., —A contribution of image processing to the diagnosis of diabetic retinopathy— Detection of exudates in color fundus images of the human retina, IEEE Transactions on Medical Imaging, vol. 21, no. 10, pp. 1236-1243, 2002

44. Zana F., and Klein J., —Segmentation of vessel-like patterns using mathematical morphology and curvature evaluation, IEEE Transactions on Image Processing, vol. 10, no. 7, pp.1010–1019, 2001

45. Jiang X., and Mojon D., —Adaptive Local Thresholding by Verification-Based Multithreshold Probing with Application to Vessel Detection in Retinal Images, IEEE Transactions on Pattern Analysis and Machine Intelligence, vol. 25, no. 1, pp. 131– 137, 2003.

46. Gregson P., Shen Z., Scott R., and Kozousek V., —Automated grading of venous beading, Computers and Biomedical Research, vol. 28, no. 4, pp. 291-304, 1995.

47. Goldbaum M., Moezzi S., Taylor A., Chatterjee S., Boyd J., and Hunter E., —Automated diagnosis and image understanding with object extraction, object classification, and inferencing in retinal images, Proceedings IEEE international conference on image processing, vol. 3, pp. 695–8, 1996.

48. Gagnon L., Lalonde M., and Beaulieu M., —Procedure to detect anatomical structures in optical fundus images, Proceedings of Conference on Medical Imaging 2001: Image Processing, vol. 4322, pp. 1218-1225, 2001.

49. Zhang E. H., and Zhang Y., —Automatic Retinal image registration based on blood vessel feature point, Proceedings of Conference on Machine learning and Cybernetics, vol. 4, pp. 2010 2015, 2002.

50. Osareh A., Mirmehdi M., Thomas B., and Markham R., — Automated identification of diabetic retinal exudates in digital colour images, British Journal of Ophthalmology, vol. 87, no. 10, pp. 1220-1223, 2007.

51. Sopharaki A., and Uyyanonvara B., —Automatic exudates detection from non-dilated diabetic retinopathy retinal image using fuzzy C means clustering, Proceedings of 3rd World Congress on Bioengineering, pp. 1-4, 2007.

52. Marios C., Ferraro J., Ecosse L., and Taylor H., —Assessment of optic disc cupping with digital fundus photographs, American Journal of Ophthalmology, vol. 140, no. 3, pp. 529-531.

53. Chaudhuri S., Chatterjee S., Katz N., Nelson M., and Goldbaum M., —Automatic detection of the optic nerve in retinal images, Proceedings of the IEEE International Conference on Image Processing, vol. 1, pp. 1–5. 1989b.

54. Lee S., Wang Y., and Lee E., —A computer algorithm for automated detection and quantification of microaneurysms and haemorrhages in color retinal images, Proceedings of SPIE Conference on Image Perception and Performance, vol. 3663, pp. 61–71, 1999.

55. Katz N., Goldbaum M., Nelson M., and Chaudhuri S., —An image processing system for automatic retina diagnosis. Proceedings of SPIE Conference on Three-Dimensional Imaging and Remote Sensing Imaging, pp. 131–137, 1988.

56. Osareh A., Mirmehdi M., Thomas B., and Markham R., —Colour morphology and snakes for optic disc localisation, Proceedings of 6th Conference on Medical Image Understanding and Analysis, pp. 21-24, 2002.

57. Lowell J., Hunter A., Steel D., Basu A., Ryder R., Fletcher E., and Kennedy L., —Optic nerve head segmentation, IEEE Transactions on Medical Imaging, vol. 23, no. 2, pp. 256–64, 2004.

58. Yulong M., and Dingru X., —Recognizing the glaucoma from ocular fundus image by image analysis, Proceedings of the IEEE International Conference of Engineering in Medicine and Biology Society", vol. 12, no. 1, pp. 178-179, 1990

59. Pinz A., Bernogger S., Datlinger P., and Kruger A., —Mapping the human retina, IEEE Transactions on Medical imaging, vol. 17, no. 4, pp. 210-215, 1998.

60. Liu Z., Opas C., and Krishnan S. M., —Automatic image analysis of fundus photograph, Proceedings of IEEE International Conference on Engineering in Medicine and Biology, vol. 2, pp. 524–525, 1997.

61. Kochner B., Schulmann D., Michaelis M., Mann G., and Englemeier K. H., —Course tracking and contour extraction of retinal vessels from colour fundus photographs: most efficient use of steerable filters for model based image analysis, Proceedings of the SPIE Conference on Medical Imaging, vol. 3338, pp. 755– 761, 1998.

62. Ege B. M., Hejlesen O. K., Larsen O. V., Moller K., Jennings B., Kerr D., and Cavan D. A., —Screening for diabetic retinopathy using computer based image analysis and statistical classification, Computer Methods Programs Biomedicine, vol. 62, no. 3, pp. 165–75, 2000.

63. Chrastek R., Wolf M., Donath K., Niemann H., Paulus D., and Hothorn T., —Automated segmentation of the optic nerve head for diagnosis of glaucoma, Journal of Medical Image Analysis, vol. 9, pp. 297–314, 2005.

64. Sanchez C. I., Hornero R., Lopez M. I., and Poza J., —Retinal image analysis to detect and quantify lesions associated with diabetic retinopathy, Proceedings

of 26th Annual International Conference of IEEE Engineering in medicine and biology society, vol. 1, pp. 1624–1627, 2004.

65. Foracchia M., Grisan E., and Ruggeri A., —Detection of optic disc in retinal images by means of a geometrical model of vessel structure, IEEE Transactions on Biomedical Engineering, vol. 23, no. 10, pp. 1189–1195, 2004.

66. Hoover A., and Goldbaum M., —Locating the optic nerve in a retinal image using the fuzzy convergence of the blood vessels, IEEE Transactions on Biomedical Engineering, vol. 22, no. 8, pp. 951–958, 2003.

67. Lalonde M., Beaulieu M., and Gangnon L., —Fast and robust optic disc detection using pyramidal decomposition and hausdorffbased template matching, IEEE Transaction on Medical Imaging, vol. 20, no. 11, pp. 1193-1200, 2001.

68. Walter T., and Klein J. C., —Segmentation of color fundus images of the human retina: detection of the optic disc and the vascular tree using morphological techniques, Medical Data Analysis, LNCS, vol. 2199, pp. 282–287, 2001.

69. Mendels F., Heneghan C., and Thiran J. P., —Identification of the Optic Disk Boundary in Retinal Images Using Active Contours,Proceedings of Irish Machine Vision Image Processing, pp. 103115, 1999.

70. Ibanez M., and Simo A., —Bayesian detection of the fovea in eye fundus angiographies, Pattern Recognition Letters, vol. 20, no. 2, pp. 229–240, 1999.

71. Ward N., Tomlinson S., and Taylor C., —Image analysis of fundus photographs, Ophthalmology, vol. 96, no. 1, pp. 80-86, 1989

72. Niemeijer M., van Ginneken B., Staal J., Suttorp-Schulten M., and Abramoff M., —Automatic detection of red lesions in digital color fundus photographs, IEEE Transactions on Medical Imaging vol. 24, no. 5, pp. 584–592, 2005.

73. Goh K. G., Hsu W., Lee Li, and Wang H., —ADRIS: An automatic diabetic retinal image screening system, Medical data mining and knowledge discovery, Physica-Verlag: Heidelberg, Germany, pp. 181-210, 2001.

74. Usher D., Dumskyj M., Himaga M., Williamson T. H., Nussey S., and Boyce J., —Automated detection of diabetic retinopathy in digital retinal images: a tool for diabetic retinopathy screening, Diabetic Medicine, vol. 21, no. 1, pp. 84-90, 2004.

75. Gardner G., Keating D., Williamson T. H., and Elliot A. T., —Automatic detection of diabetic retinopathy using an artificial neural network: a screening tool, British Journal of Ophthalmology, vol. 80, no. 11, pp. 940–944, 1996.

76. Jayakumari C., and Santhanam T., — Detection of Hard Exudates for Diabetic Retinopathy using Contextual Clustering and Fuzzy art Neural network, Asian Journal of Information Technology, vol. 6, no. 8, pp. 842-846, 2007.

77. Sopharak A., Uyyanonvara B., Barman S., and Williamson H. T., —Automatic detection of diabetic retinopathy exudates from nondilated retinal images using mathematical morphology methods, Computerized Medical Imaging and Graphics, vol. 32, no. 8, pp. 720-727, 2008.

78. Sopharak A., Uyyanonvara B., and Sarah B., —Automatic exudate detection from non-dilated diabetic retinopathy retinal images using fuzzy c-means clustering, Sensors, vol. 9, no. 3, pp. 21482161, 2009.

79. Sinthanayothin C., Boyce J. F., Williamson T. H., Cook H. L., Mensah E., Lal S., and Usher D., —Automated detection of diabetic retinopathy on digital fundus images, Diabetic medicine, vol. 19, no. 2, pp. 105-112, 2002.

80. Lee S., Lee E., Kingsley R., Wang Y., Russell D., Klein R., and Warn A., —Comparison of diagnosis of early retinal lesions of diabetic retinopathy between a computer and human experts, Archives of Ophthalmology, vol. 119, no. 4, pp. 509–515, 2001.

81. Fleming D. A., Philip S., Goatman A. K., and Williams J. G., Olson A. J., Sharp F. P., —Automated detection of exudates for diabetic retinopathy screening, Physics in Medicine and Biology, vol. 52, no. 24, pp. 7385-7396, 2007.

82. Estabridis K., and de Figueiredo R. J. P., —Automatic Detection and Diagnosis of Diabetic Retinopathy, IEEE International Conference on Image Processing, ICIP, vol. 2, pp. 445-448, 2007.

83. Nayak J., Bhat P. S., Acharya U. R., Lim C. M., and Kagathi M., —Automated Identification of Different Stages of Diabetic Retinopathy using digital fundus images, Journal of Medical Systems, vol. 32, no. 2, pp. 107-115, 2008.

84. Nayak J., Bhat P. S., and Acharya U. R., —Automatic identification of diabetic maculopathy stages using fundus images, Journal of Medical Engineering Technology vol. 33, no. 12, pp. 119-129, 2009.

85. Sinthanayothin C., Kongbunkiat V., Phoojaruenchanachai S., and Singalavanija A., —Automated Screening System for Diabetic Retinopathy, Proceedings of the 3rd International Symposium on Image and Signal Processing and Analysis , pp. 915- 920, 2003.

86. Liu Z. Q., Rangayyan R. M., and Frank C. B., —Analysis of directional features in images using gabor filters, 3rd Annual IEEE Symposium on Computer Based Medical Systems, USA, pp, 68-74, 1990.

87. Daugman J. G., —Complete discrete 2-D Gabor transforms by neural networks for image analysis and compression, IEEE Transactions on Acoustics, Speech, Signal Processing, vol. 36, no. 7, pp. 1169-1179, 1988.

88. Manjunath B. S., and Ma W. Y., —Texture features for browsing and retrieval of image data, IEEE Transactions on Pattern Analysis and Machine Intelligence, vol. 18, no. 8, pp. 837–842, 1996.

89. Liu Z. Q., Cai J., and Buse R., —Hand-writing Recognition: Soft Computing and Probablistic Approaches, Springer Verlag, Berlin, 2003.

90. Lee T. S., —Image representation using 2D Gabor wavelets, IEEE Transactions of Pattern Analysis and Machine Intelligence, vol. 18,no. 10, pp. 959-971, 1996.

91. Chen J., Sato Y., and Tamura S., —Orientation space filtering for multiple orientation line segmentation, IEEE Transactions of Pattern Analysis and Machine Intelligence, vol.22, pp.417-429, 2000.

92. Mark L. G. A., and Chein C., —Target detection in multispectral images using the spectral co-occurrence matrix and entropy thresholding, Optical Engineering, vol. 34, no. 7, pp. 2135-2148, 1995.

93. Mokji M., S. A. R., and Abu B., —Adaptive thresholding based on co-occurrence matrix edge information, Journal of Computers, vol. 2, no. 8, pp. 44-52, 2007.

94. Hoover A., Kouznetsoza V., and Goldbaum M., —Locating blood vessels in retinal images by piecewise threshold probing of a matched filter response, IEEE Transactions on Medical Imaging, vol. 19, no. 3, pp. 203–210, 2000.

95. Quigley H. A., —Number of people with glaucoma worldwide, British Journal of Ophthalmology, vol. 80, no. 5, pp. 389–393, 1996.

96. Kass M., Witkin A., and Terzopoulos D., —Snakes: active contour models, International Journal on Computer Vision, vol. 1, no. 4, pp. 321–331, 1987.

Appendix A

LIST OF PUBLICATIONS

1. Sangramsing N.Kayte ,Dr Ramesh R.Manza "Automatic detection Non-proliferative Diabetic Retinopathy Detection Technique using Image Features Extraction Techniques" International Journal of Engineering Research and Applications (IJERA) 6 july2013

2. Sangramsing N. Kayte Siddharth B. Dabhade, Bharatratna P. Gaikwad,"Design and Development for Detection of Blood Vessels, Microneurysms and Exudates from the Retina, Proceedings of the National Conference on Advancements in the Era of Multi- Disciplinary Systems (AEMDS-2013), Elsevier Publications 2013,ISBN: 978-93-5107- 057-3,pp.394-402